-1

DOT-CG-D-02-87
DOT-TSC-CG-87-1

GPS Field Test Data Analysis

John H. Kraemer

Transportation Systems Center
Cambridge, MA 02142

December 1986
Final Report

Office of Research and Development
Systems Technology Division
Washington DC 20593

Technical Report Documentation Page

1. Report No.	2 Government Accession No	3. Recipient's Catalog No.
DOT-CG-D-02-87		

4. Title and Subtitle	5. Report Date
GPS FIELD TEST DATA ANALYSIS	December 1986
	6. Performing Organization Code: DTS-52
7. Author(s): John H. Kraemer	8. Performing Organization Report No.: DOT-TSC-CG-87-1
9. Performing Organization Name and Address: U.S. Department of Transportation, Research and Special Programs Administration, Transportation Systems Center, Cambridge, MA 02142	10. Work Unit No (TRAIS): CG745/B7006
	11. Contract or Grant No.
12. Sponsoring Agency Name and Address: U.S. Department of Transportation, United States Coast Guard, Office of Research and Development, Washington, DC 20593	13. Type of Report and Period Covered: Final Report, June 1984 - August 1984
	14 Sponsoring Agency Code: G-DST-1

15. Supplementary Notes

16. Abstract

This report discusses the analysis of GPS measurement data gathered under the joint sponsorship of the Defense Mapping Agency (DMA) and the National Oceanic and Atmospheric Administration (NOAA). The DMA/NOAA data have been made available to TSC in support of the Coast Guard's interest in using Differential GPS for civil marine applications. Pseudorange measurements gathered simultaneously at two or more sites are processed differentially in order to determine the effectiveness of Differential GPS in reducing system bias errors. The results obtained show a significant reduction in bias errors as a consequence of differential processing. Mean horizontal differential errors on the order of one part in 100,000 were noted over site separations ranging from 276 to 1,591 kilometers.

17. Key Words	18. Distribution Statement
NAVSTAR, GPS. Differential GPS, TI-4100, VLBI, Ionospheric, Tropospheric	DOCUMENT IS AVAILABLE TO THE PUBLIC THROUGH THE NATIONAL TECHNICAL INFORMATION SERVICE, SPRINGFIELD VIRGINIA 22161

19. Security Classif. (of this report)	20 Security Classif (of this page)	21. No. of Pages	22. Price
UNCLASSIFIED	UNCLASSIFIED	162	

Form DOT F1700.7 (8-72) Reproduction of completed page authorized

PREFACE

This report discusses the analysis of GPS measurement data gathered under the joint sponsorship of the Defense Mapping Agency (DMA) and the National Oceanic and Atmospheric Administration (NOAA). The DMA/NOAA data have been made available to the Transportation Systems Center (TSC) in support of the Coast Guard's interest in using Differential GPS for civil marine applications. Pseudorange measurements gathered simultaneously at two or more sites are processed differentially in order to determine the effectiveness of Differential GPS in reducing system bias errors. The results obtained show a significant reduction in bias errors as a consequence of differential processing. Mean horizontal differential errors on the order of one part in 100,000 were noted over site separations ranging from 276 to 1,591 kilometers.

CONTENTS

LIST OF FIGURES

LIST OF FIGURES (CONTINUED)

LIST OF FIGURES (CONTINUED)

1. INTRODUCTION

This report discusses the analysis of GPS measurement data gathered under the joint sponsorship of the Defense Mapping Agency (DMA) and the National Oceanic and Atmospheric Administration (NOAA). The DMA/NOAA data have been made available to TSC in support of the Coast Guard's interest in GPS for civil marine applications. Broadly speaking, these interests cover two specific applications. These are:

1. Differential L_1 C/A (non-military) code operation with pseudorange/range rate corrections provided from a reference site or a pseudolite.
2. Stand-alone operation using the L_1 C/A code only.

Differential operation has the potential to satisfy the stringent 8-20 meter, 2 drms accuracy requirements for the Harbor and Harbor Approach phases of navigation using the Standard Positioning Service. Differential GPS involves the use of a GPS monitor receiver located at an accurately surveyed benchmark. The monitor receiver measures fixed or slowly-varying GPS system bias errors. These measured bias values are broadcast to remote users where they are used to remove the GPS system bias errors at the remote receiver. Field data, gathered simultaneously at two or more sites, provides a means by which range corrections derived for one site can be applied to the range measurements of one or more remote sites to determine the effectiveness of differential operation. The results reported herein must, however, be qualified. For national security reasons the Department of Defense plans to degrade the accuracy of the C/A code under a program called Selective Availability (SA) to be included in the

2. BACKGROUND

The DMA/NOAA GPS field tests were conducted in CY 1984 using two-frequency, P-code receivers developed for DMA/NOAA by Texas Instruments, Inc. The DMA/NOAA receiver is a four-channel, fast multiplexed set whose commercial version is the TI 4100 NAVSTAR Navigator. Measurements were made at accurately surveyed, fixed locations in California, Alaska and Canada. The California tests were made during January and February 1984 when satellite visibility was confined to the nighttime when the ionospheric activity was minimal. Alaska/Canada data were gathered under daytime conditions during July and August 1984. Data recording typically began around 1:00 PM local time and lasted from two to four hours. Thus, the Alaska/Canada data can be expected to span conditions of peak diurnal ionospheric activity.

The primary objective of the data analysis conducted during this reporting period is to evaluate the potential effectiveness of Differential GPS in minimizing the effects of GPS system bias errors. The two most important bias errors for the single-frequency C/A code user are expected to be Selective Availability (SA) and unmodeled signal propagation delays. Since Selective Availability is not yet operational, the results presented apply principally to unmodeled propagation delays. Here, we are concerned with the departure of the actual delay from that predicted by the single-frequency ionospheric model supported by the GPS data message and by the simple tropospheric delay model developed by Edward E. Altshuler. (2) Of the two effects, the ionospheric delay is the more difficult to model. Klobuchar (3) estimates that the ionospheric model will only correct for approximately 50 percent of the ionospheric time delay on an rms basis. One of the major limitations in the use of the ionospheric model is that while it is reasonably effective in reducing errors in

3. SOFTWARE DESCRIPTION

Four major pieces of software have been developed for the analysis of the DMA/NOAA field test data. Two of these software packages, the single receiver program and the propagation model program, have already been described in Section 3 of the previous Project Memorandum. (1) The single receiver program is used to analyze data from a single receiver operated in a "stand-alone" configuration. Computed navigation position solutions are compared with the known coordinates of the receiver (the phase center of the antenna) and errors in latitude and longitude are computed. The propagation model software is intended to be used to compare the ionospheric and tropospheric model predictions with measured data. In the case of the ionospheric model, the single-frequency model prediction is compared with values determined from two frequency (L_1 and L_2) P-code measurements. Since, to a first order, the ionospheric delay is related to the inverse square of the carrier frequency, the L_1 and L_2 pseudoranges provide a direct measure of ionospheric delay. Because we have no direct way of measuring the tropospheric delay, our initial intent was to subtract the measured two-frequency ionospheric delay from the measured range and assume that the remaining delay was due to the troposphere. This approach was not feasible, since the magnitude of the GPS system bias often exceeded that of the tropospheric model uncertainty.

3.1 DIFFERENTIAL GPS SOFTWARE

The Differential GPS software is used to process measurements from two physically separated GPS receivers in a differential mode. Figure 3-1 shows the overall data processing in block diagram form. The left-hand side of the block diagram shows the basic processing that is done at both the reference site and at the mobile site. Details of this basic processing are given in reference (1)

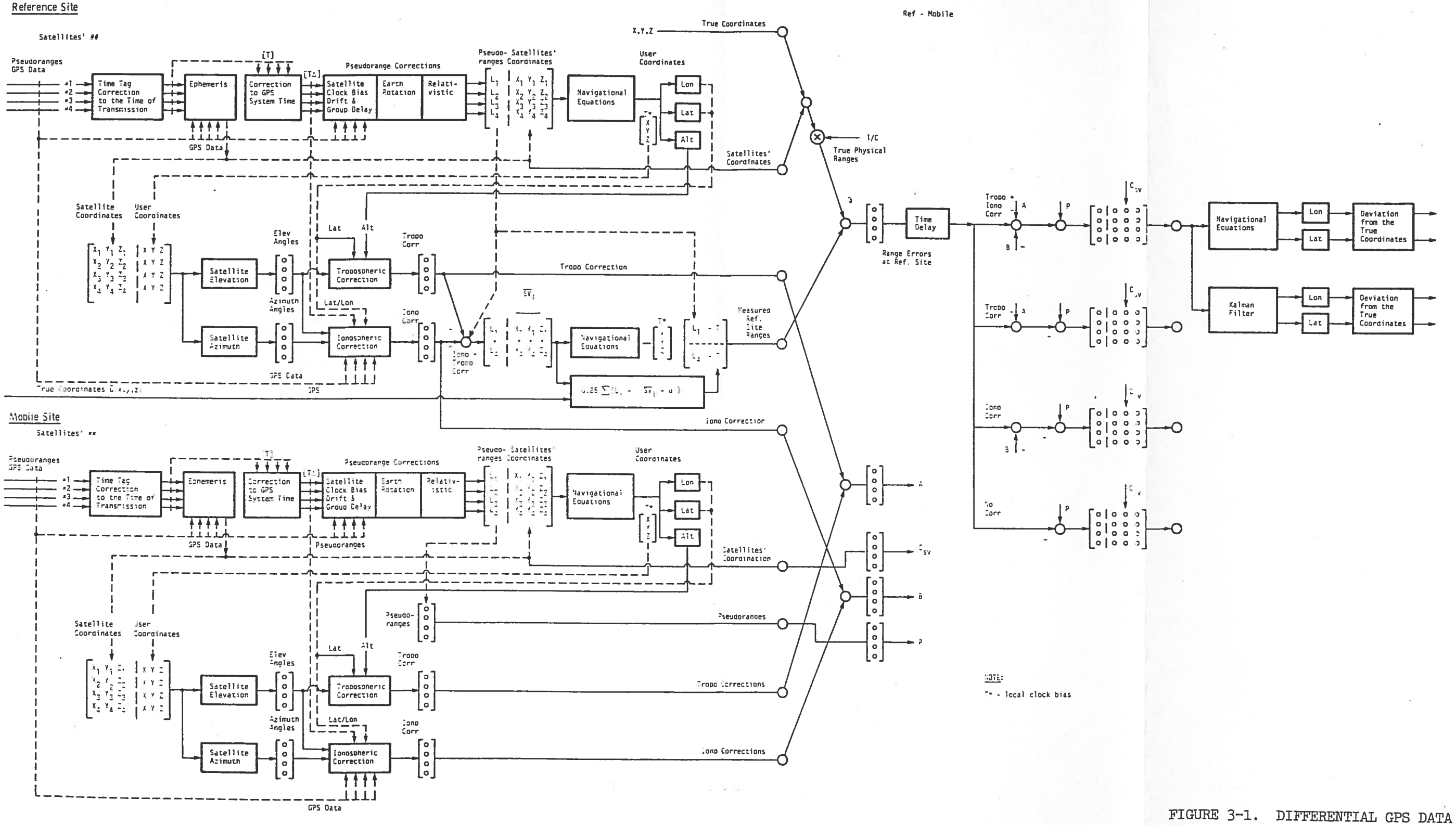

FIGURE 3-1. DIFFERENTIAL GPS DATA PROCESSING

For example, if the reference site were at a much higher altitude than the mobile site, its measured corrections would fail to account for the added tropospheric delay experienced by the mobile site. Use of a tropospheric model difference (reference minus mobile) would provide an estimate of the additional correction required at the mobile site.

The top line on the right-hand side of Figure 3-1 shows the processing for the application of both tropospheric and ionospheric model differences to the reference site range error corrections. The second, third, and fourth lines correspond to use of tropospheric model differences, ionospheric model differences, and neither, respectively. In the bottom line the reference site corrections are applied without any model corrections. The resulting corrected pseudoranges are used as inputs to the Navigation Equations which are solved for the position coordinates and clock bias of the mobile site receiver. Position solutions are computed for the four possible combinations of model corrections.

While the block diagram of Figure 3-1 shows the overall data processing scheme for Differential GPS, it doe not correspond directly to the Differential GPS software. The actual data processing is done by running the Single Receiver software twice, once for the "reference site" and once for the "mobile site." The Single Receiver software creates output files containing not only the single-receiver position errors, but also the results of various intermediate computations, including the tropospheric and ionospheric delays. The Differential GPS software reads these single-receiver files and creates an output file containing the results of the differential processing. Thus, error plots can be obtained for each station acting alone as well as in combination, with either serving as the reference site. No distinction is made between reference site and mobile site at the time of data recording.

4. DATA ANALYSIS

This section presents an analysis of data from the DMA/NOAA tests of January-February 1984 and of NOAA sponsored tests conducted in Alaska and Canada during the summer of 1984. The DMA/NOAA tests were made using very long baseline interferometer (VLBI) sites in California. Since the VLBI tests were made during nighttime, the ionospheric delay can be expected to be at a diurnal minimum with little, if any, spatial variation. Thus, examples of differential processing of these data will tend to be overly optimistic. Data from the NOAA Alaska/Canada tests was gathered during the early- and mid-afternoon when ionospheric activity can be expected to reach its maximum. Differential processing of these data sets should be more representative of the potential effectiveness of Differential GPS.

All of the results presented in this report are based upon use of the P-code on the L_1 frequency. Results are based upon so-called "point solutions" computed from a single set of four pseudoranges without any data averaging. For this reason, the results can be considered to be somewhat conservative insofar as they relate to random variations. It is important to note, however, that slowly-varying bias errors would be unaffected by data smoothing. In this regard the results shown can be considered representative of what might be achieved with differential processing. It should also be pointed out that all results presented in this report are based upon measurements made at fixed locations.

4.1 ANALYSIS OF CALIFORNIA VLBI SITE DATA

Data sets are identified by the Julian day on which the test was conducted and by the name of the VLBI site where the GPS receiver was located.

TABLE 4-1. DIFFERENTIAL PROCESSING OF VLBI DATA SETS

DAY	REFERENCE SITE LAT/LONG/HGHT	TIMETAG CORRECTION (ms)	REMOTE SITE LAT/LONG/HGHT	TIMETAG CORRECTION (ms)	BASELINE (km)
017	HARVARD 30° 38' 9.44557" 256° 3' 10.36579" 1,583.45 m	8.35	VENUS 35° 14' 533.11116" 243° 12' 27.35881" 1,037.93 m	23.00	1,302.3
029	BARSTOW 35° 5' 27.01699" 243° 3' 38.42713" 1,363.17 m	-0.625	VENUS (see above)	0.0	22.0
029	MOJAVE 35° 19' 48.99710" 243° 6' 31.21268" 913.69 m	0.0	BARSTOW (see above)	-0.625	26.9
029	VENUS (see above)	0.0	MOJAVE (see above)	0.0	12.7
031	POINT 34° 27' 13.60196" 242° 55' 55.11976" 905.20 m	0.0	VENUS (see above)	0.0	91.7

The offsets of the phase center of the antenna from the mark are:

0.000 meters north

0.000 meters east

1.529 meters above ref. ellipsoid

Harvard (site number 85032)

Latitude: 30 degrees, 38 minutes, 9.44557 seconds

Longitude: 256 degrees, 3 minutes, 10.36579 seconds

Height: 1.58345 kilometers above ref. ellipsoid

X = -1324.205363 kilometers

Y = -5332.057052 kilometers

Z = 3232.038414 kilometers

The offsets of the phase center of the antenna from the mark are:

0.000 meters north

0.000 meters east

1.350 meters above ref. ellipsoid

The time interval between observations is 12 seconds, so that a one minute time interval is represented by an observation number change of five. Timetag/pseudorange corrections of 23.00 and 8.35 milliseconds were applied to the Venus and Harvard data sets, respectively.

4.1.1.1 Satellite Geometry, Harvard Site - Figure 4-1 shows the geometry of the satellite constellation as seen from the Harvard site during the data analysis interval. The data analysis interval for the Harvard data is from t(GPS) = 211,968 seconds (obs. no. 001) to t(GPS) = 219,624 seconds (obs. no. 639). As can be seen from the figure, SV 9 (space vehicle nine) has an elevation angle of

7 degrees above the user's horizon at the beginning of the test and reaches an elevation angle of 64 degrees at the end of the measurement sequence. The corresponding elevations for SVs 6, 8 and 11 are 48/64, 62/7 and 63/51 degrees, respectively. The initial geometry of the constellation with respect to the user is relatively favorable. As time increases, the geometry becomes progressively worse until late in the pass when the geometry begins to improve again. The various dilution of precision measures for the Harvard site are shown in Figure 4-2. HDOP remains between 3.9 and 6.0 during the first 217 observations (43 minutes). Satellite geometry becomes singular at observation number 331. HDOP then falls to 6.0 at observation number 447 and remains between 6.0 and 4.2 for the remaining 38 minutes of the run. Since the HDOP algorithm had not been implemented at the time many of the computations were made, the magnitude of the determinant of the solution matrix was used initially as a measure of the influence of geometric effects on solution accuracy. As the determinant of the solution matrix approaches zero, HDOP becomes unbounded and the solution "blows up." Small values of the magnitude of the determinant of the solution matrix correspond to large values of HDOP and consequently to large solution errors. The magnitude of the determinant of the solution matrix appears on plots of horizontal position error which follow.

4.1.1.2 User Position Errors, Harvard Site - Figure 4-3 shows a plot of the horizontal position error as a function of observation number. The computation of position involves the use of both ionospheric and tropospheric propagation models. Horizontal position error remains below 16.2 meters during the first 217 observations for which HDOP is less than or equal to 6.0. It then increases abruptly as the geometry becomes singular at observation number 331. The error then decreases, falling to below 17.7 meters for the last portion of the run for

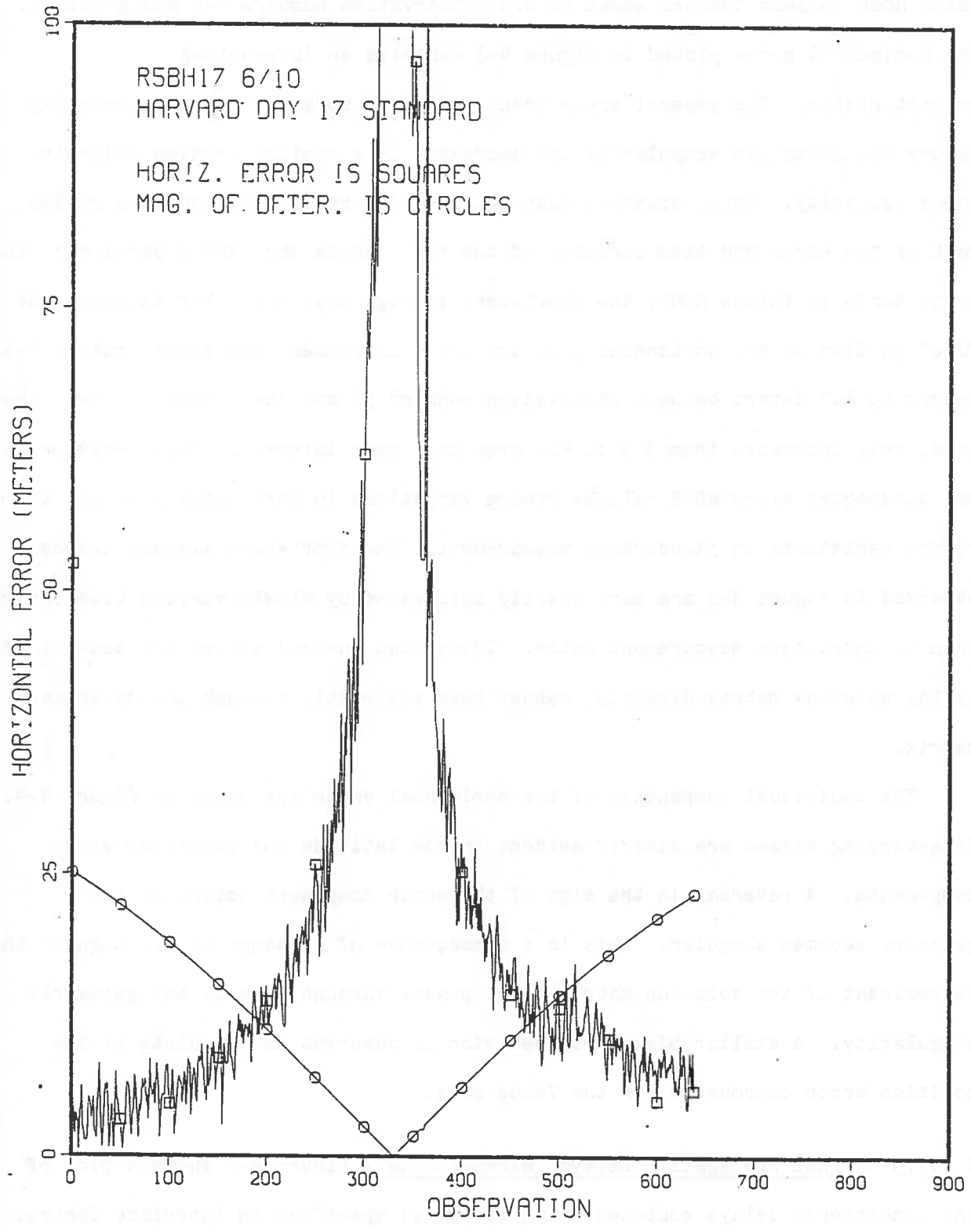

FIGURE 4-3. HORIZONTAL POSITION ERROR, DAY 017, HARVARD SITE

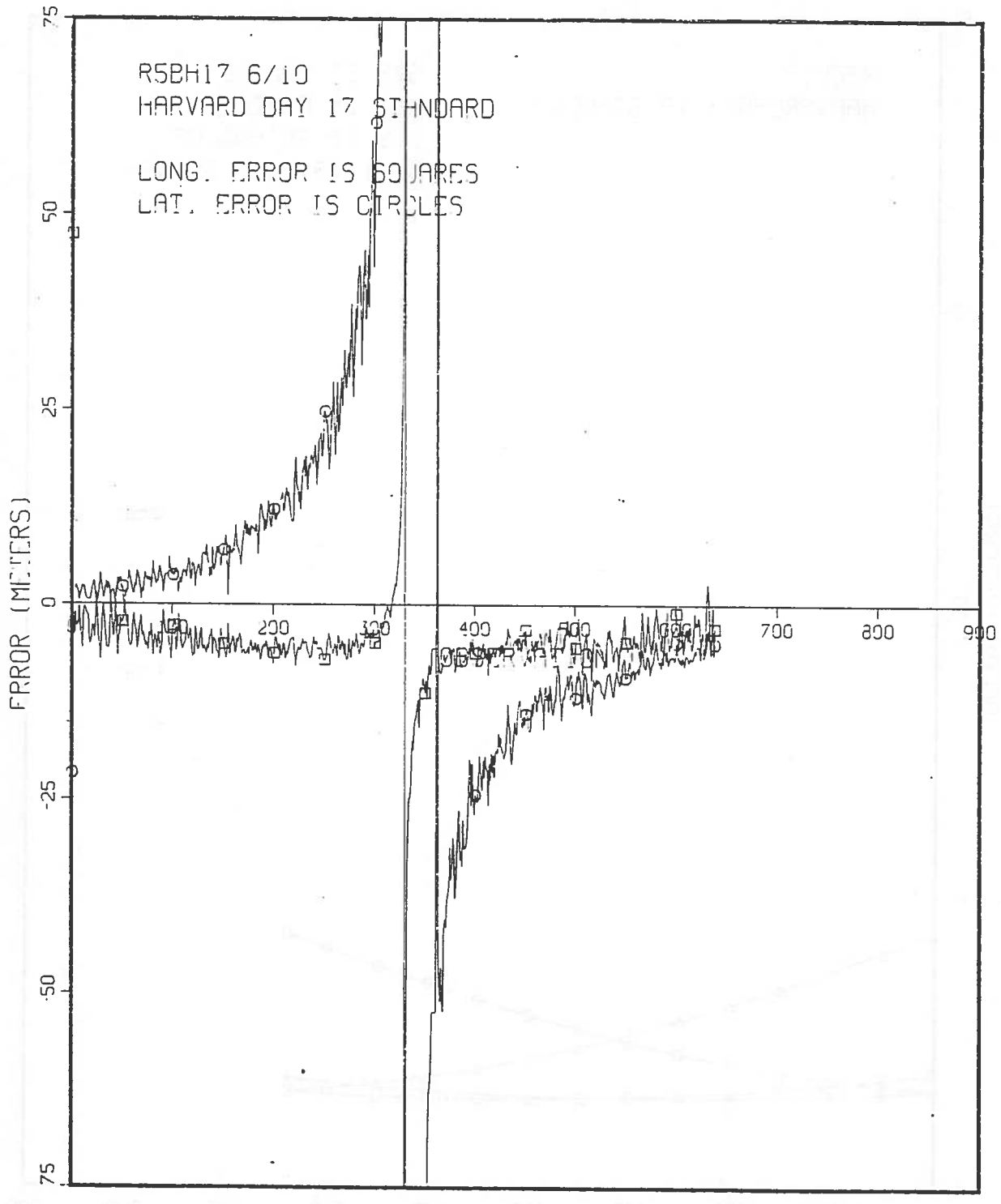

FIGURE 4-4. ERROR COMPONENTS, DAY 017, HARVARD SITE

values were taken from a table provided by Space Division/OL-AQ/GPS Vandenberg AFB. The four beta coefficients given in the table must be divided by 2 Π prior to their being used in the algorithm specified in ICD-GPS-200. (4) This requirement was pointed out to TSC by Dr. Javad Ashjaee of Trimble Navigation. Solar flux values used by the model were provided by John Klobuchar of the Air Force Geophysics Laboratory, Hanscom AFB. A five day average of the solar flux was used at the suggestion of Mr. Klobuchar. Delays for SVs 6 and 11 remain below 2 meters while delays for SVs 8 and 9 range between approximately 1.5 to 4.5 meters. The trends follow expectations. The SV 9 delay has an initial value of 4.34 meters, and it falls monotonically to a final value of 1.63 meters. This is consistent with its elevation angle which starts out at 7.0 degrees and increases to a final value of 63.6 degrees. Similarly, the delay associated with SV 8 increases monotonically from an initial value of 1.66 meters to a final value of 4.34 meters. The elevation angle of SV 8 decreases monotonically from an initial value of 61.9 degrees to a final value of 7.0 degrees. Ionospheric delays for SV 6 and SV 11 reach their minimum values during the run. This is consistent with their reaching their maximum elevation angles during the run. Since the measurements were taken under conditions of darkness, the ionospheric shell is modeled as being of a constant thickness and hence the obliquity factor is the only variable. The obliquity factor accounts for the increasing ionospheric path length with decreasing elevation angle. Variation of the ionospheric obliquity factor with SV elvation angle is given in Table 4-2.

Figure 4-6 shows a plot of the tropospheric delays computed using the model described in reference (2). The behavior shown is similar to that observed in Figure 4-5 for the ionospheric delays. This also is consistent with expectations. The ionospheric and tropospheric models follow a somewhat similar

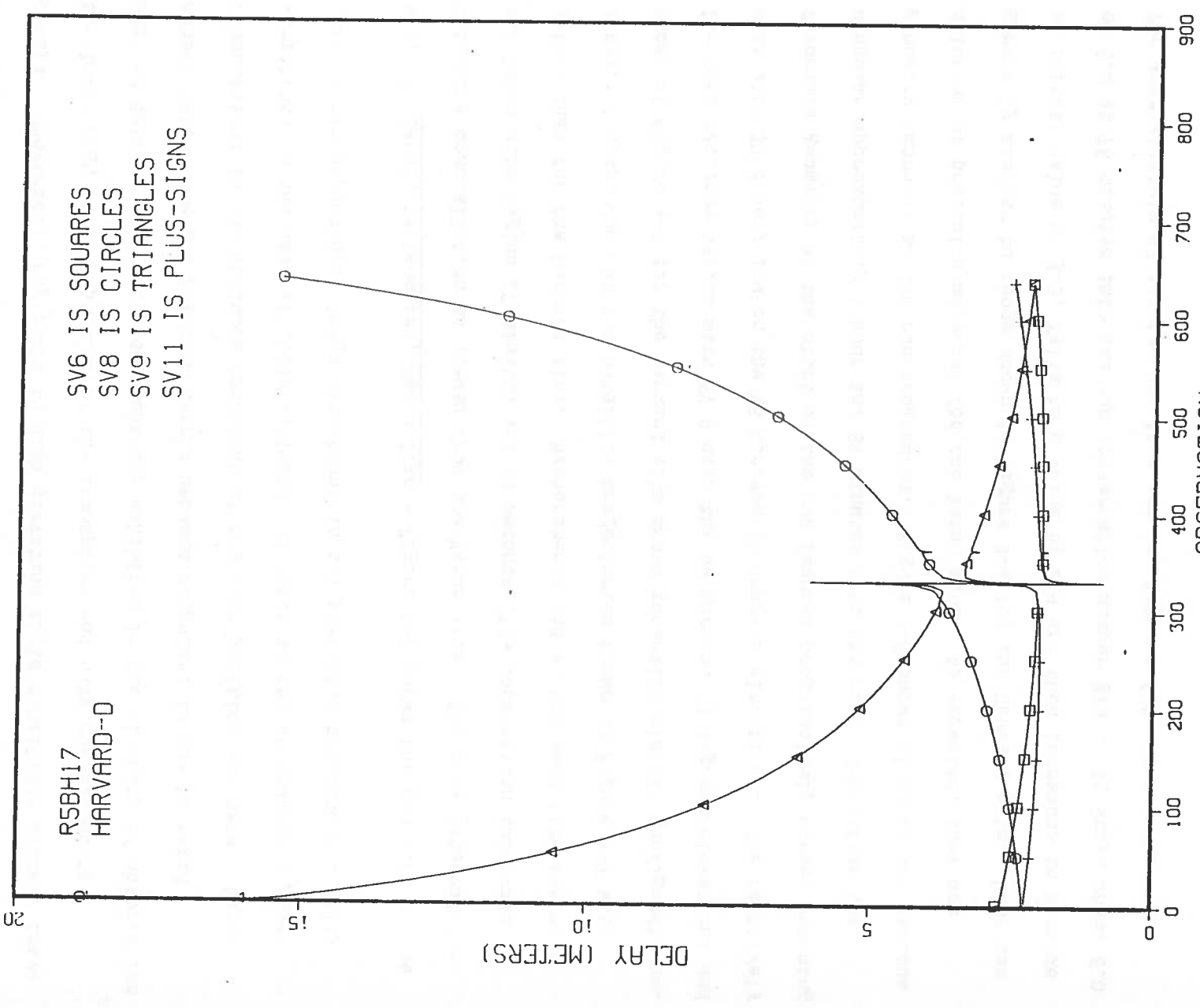

FIGURE 4-6. COMPUTED TROPOSPHERIC DELAY, DAY 017, HARVARD SITE

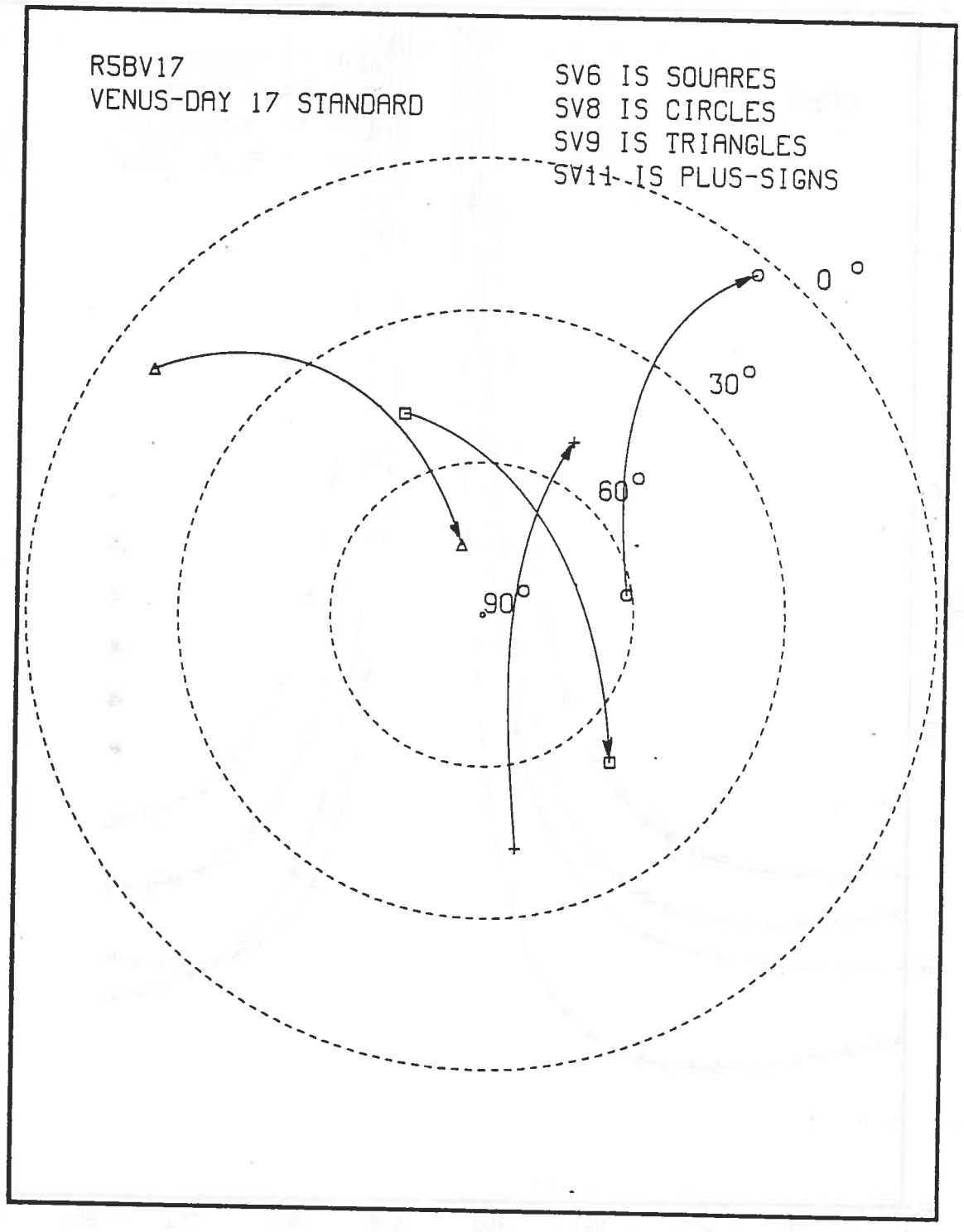

FIGURE 4-7. SATELLITE GEOMETRY, DAY 017, VENUS SITE

the remainder of the run. Thus, HDOP is somewhat lower at Venus than at Harvard before the singularity in geometry and somewhat higher than that at Harvard following the singularity.

4.1.1.5 User Position Error, Venus Site - Horizontal position error is shown in Figure 4-9. As in the case of the companion plot (Figure 4-3) for the Harvard site, pseudoranges have been corrected for both tropospheric and single-frequency ionospheric error models. The general features of the two plots are seen to be quite similar when one allows for the fact that the Venus plot begins 139 observation numbers (27 minutes, 48 seconds) before the Harvard plot. Random variations are more evident in the Harvard data at the beginning of the run, while peak-to-peak excursions are somewhat greater in the Venus data in the last half of the run. Since carrier-to-noise power density ratios were not recorded, no readily available measure of signal quality is available for site-to-site comparison.

Figure 4-10 shows the individual components of the horizontal position error for the Venus site. Taking the relative starting times into account, it can be seen that the general trends of the error components at the Harvard and Venus sites are quite similar. The large error spikes at observation number 362 in the Venus data are not of great significance, as they would normally be rejected through a combination of data editing/smoothing.

4.1.1.6 Signal Propagation Delays, Venus Site - Figure 4-11 shows a plot of the ionospheric delays computed using the single-frequency ionospheric correction model. The model used the same five day average of the solar flux values as were used for the Harvard data (Figure 4-5). The general features of the plots for the Venus site are similar to those for the Harvard site, reflecting the

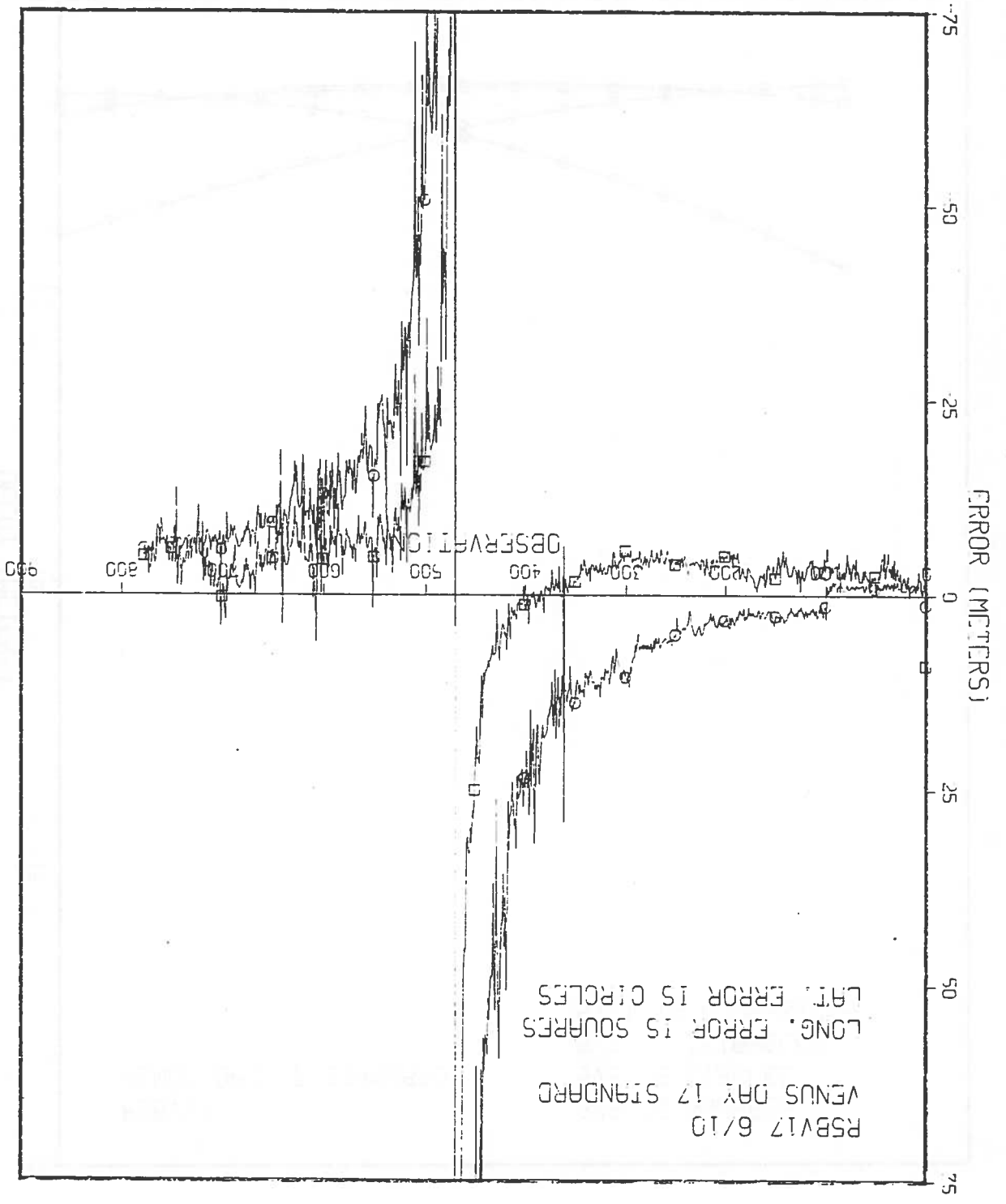

FIGURE 4-10. ERROR COMPONENTS, DAY 017, VENUS SITE

similarity of satellite geometry as observed at the two sites. Figure 4-12 shows a plot of the computed tropospheric delay for the Venus site. The delay profiles shown are very similar to those given for Harvard in Figure 4-6. Note that the larger initial value for SV 9 (16.0 meters) at Harvard is consistent with its lower initial elevation angle at Harvard as compared to Venus. Similarly, the SV 8 final delay for Venus is larger than that for Harvard. This corresponds to the lower elevation angle of SV 8 as seem from the Venus site at the end of the run. The dramatic change in tropospheric delay near the horizon is quite evident in these plots. The sharp spike in the tropospheric data at observation number 469 (Figure 4-12) corresponds to a large altitude uncertainty associated with the singular SV geometry.

4.1.1.7 Differential Operation - The horizontal error plot shown in Figure 4-13 shows the error reduction achieved through differential processing of the data from the Harvard and Venus sites. Harvard served as the reference site. Pseudorange corrections from the Harvard site were compensated for tropospheric and ionospheric model differences (Harvard minus Venus) and applied to pseudoranges measured at the Venus site. The time span shown in Figure 4-13 is the same as that shown in Figure 4-3 for the Harvard site since that is the interval over which data were measured at both sites. Although the data shown in Figure 4-13 may appear quite noisy, it should be noted that there is a four-to-one scale change between Figure 4-13 (25 meters full scale) and companion single-receiver plots for Harvard (Figure 4-3) and Venus (Figure 4-9) where full scale equals 100 meters. Moreover, since the reference site corrections are unfiltered, the random noise power associated with the Harvard measurements is added to that of the Venus measurements in the differential data presented in Figure 4-13. The most notable feature of the plot shown in Figure 4-13 is a

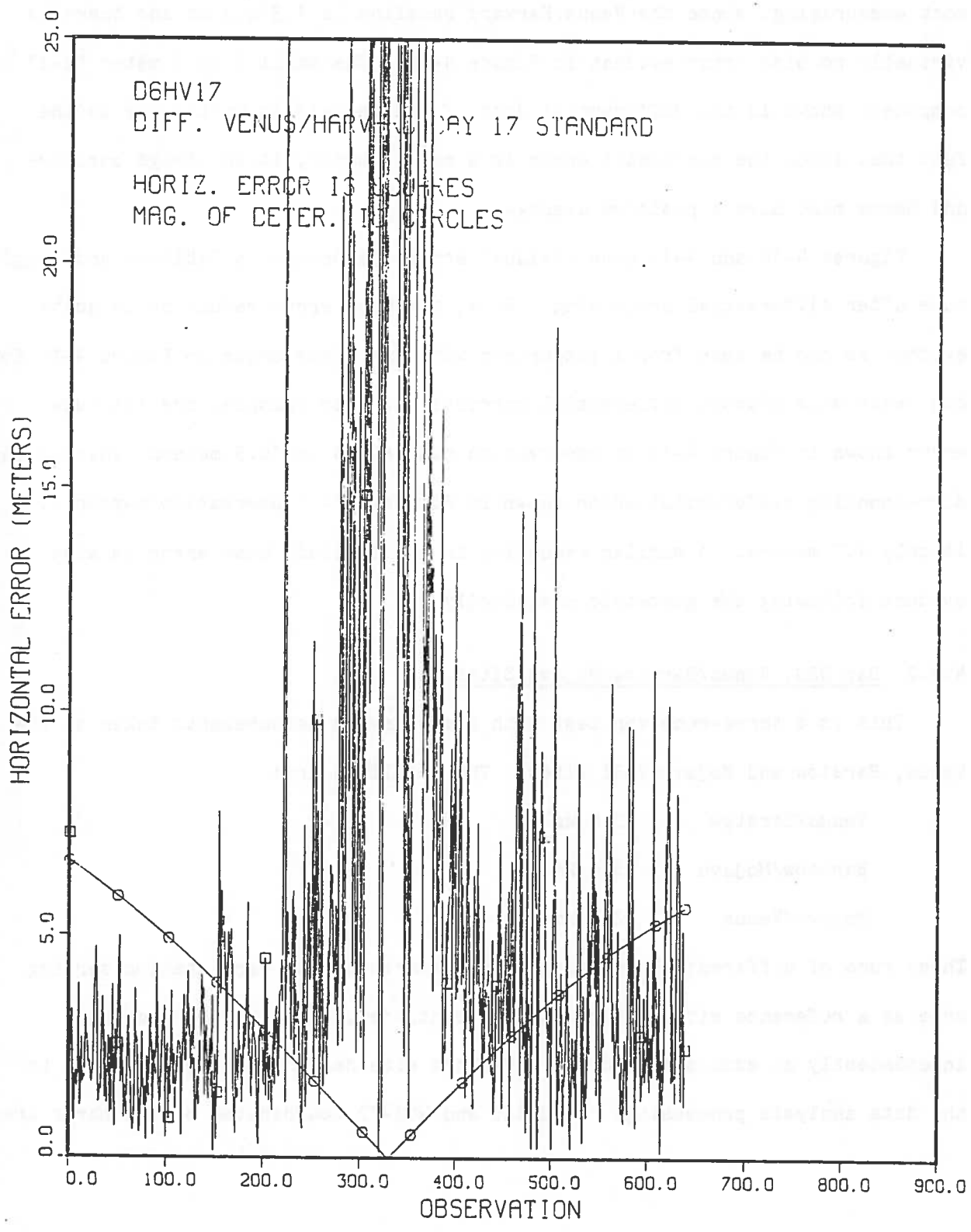

FIGURE 4-13. HORIZONTAL DIFFERENTIAL ERROR, DAY 017, VENUS/HARVARD BASELINE

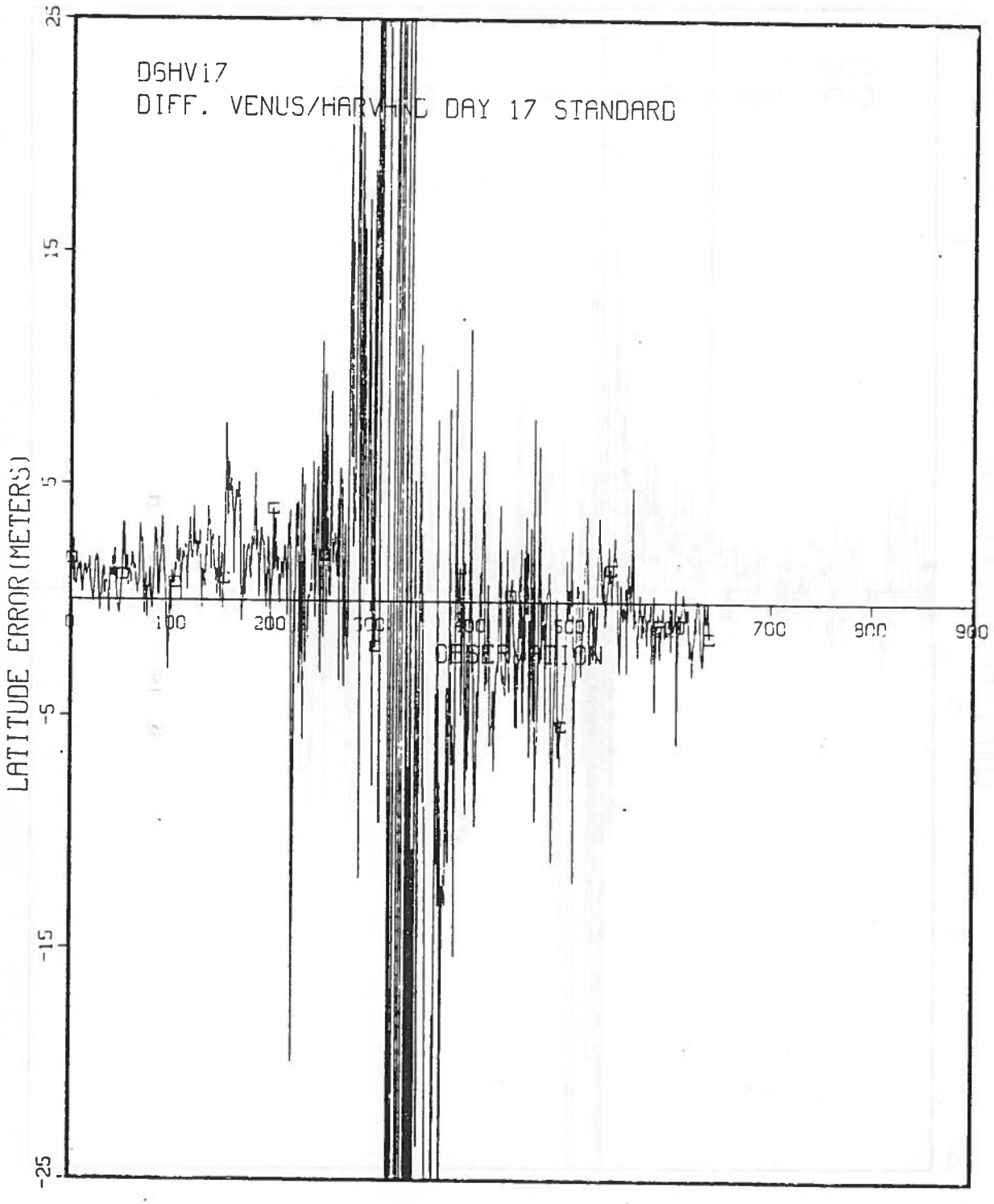

FIGURE 4-14. DIFFERENTIAL ERROR LATITUDE COMPONENT, DAY 017, VENUS/HARVARD BASELINE

Venus (site number 85031)

Latitude: 35 degrees, 14 minutes, 53.11116 seconds

Longitude: 243 degrees, 12 minutes, 27.35881 seconds

Height: 1.037937 kilometers above ref. ellipsoid

X = -2350.906034 kilometers

Y = -4655.537189 kilometers

Z = 3660.976579 kilometers

The offsets of the phase center of the antenna from the mark are:

0.000 meters north

0.000 meters east

1.529 meters above ref. ellipsoid

Barstow (site number 85036)

Latitude: 35 degrees, 5 minutes, 27.01699 seconds

Longitude: 243 degrees, 3 minutes, 38.42713 seconds

Height: 1.36317 kilometers above ref. ellipsoid

X = -2367.510466 kilometers

Y = -4658.690347 kilometers

Z = 3646.900197 kilometers

The offsets of the phase center of the antenna from the mark are:

0.000 meters north

0.000 meters east

1.379 meters above ref. ellipsoid

Mojave (site number 85035)

Latitude: 35 degrees, 19 minutes, 48.99710 seconds

Longitude: 243 degrees 6 minutes, 31.21268 seconds

Height: 0.91369 meters above ref. ellipsoid

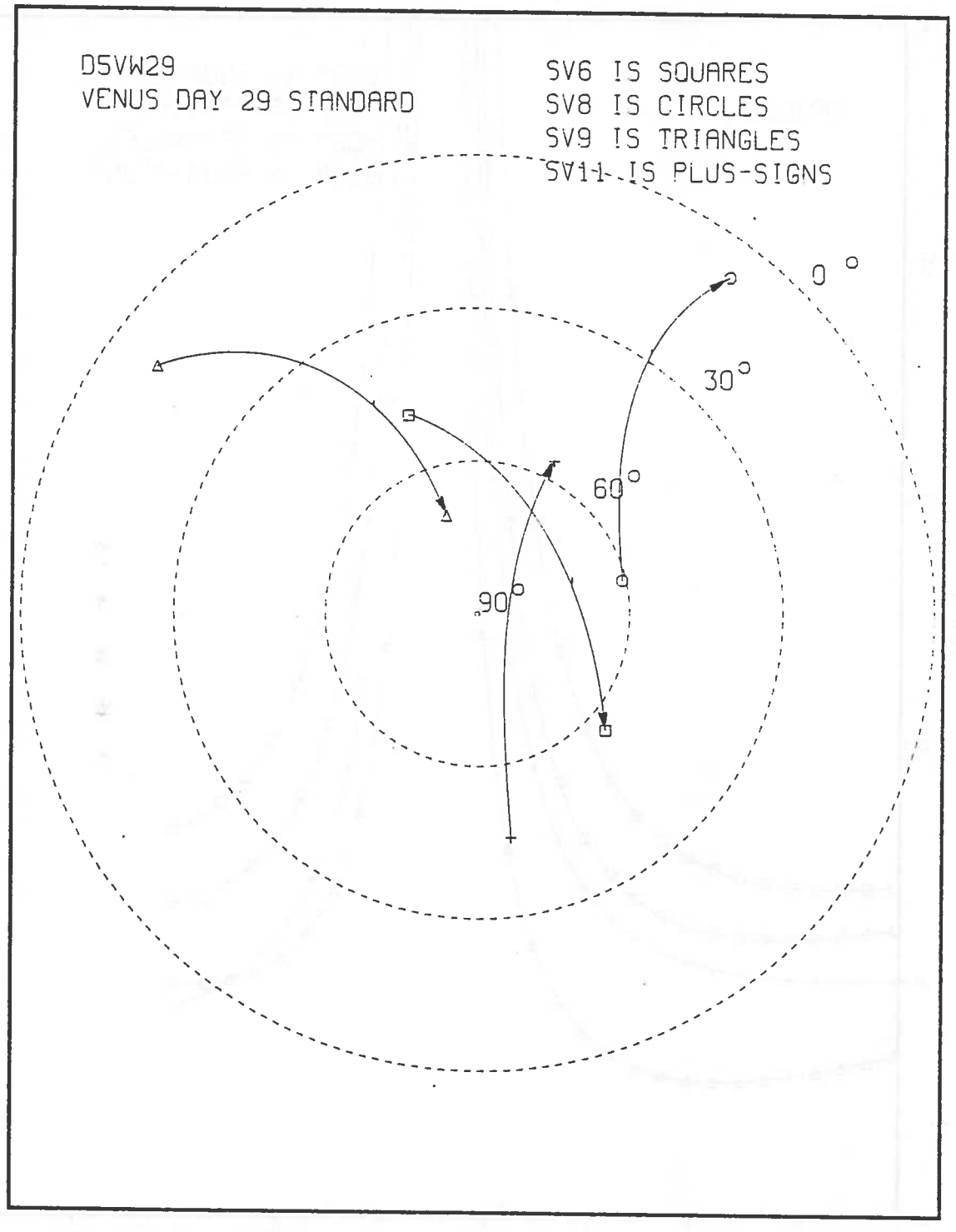

FIGURE 4-16. SATELLITE GEOMETRY, DAY 029, VENUS SITE

sites. A comparison of Figure 4-17 with Figure 4-8 (Venus, Day 017) shows close agreement. This is to be expected, since the satellite geometry is periodic for a given site, repeating every 23 hours, 56 minutes, 4.09 seconds. Therefore, the comments made in the previous section for Day 017 (Venus Site) satellite geometry apply equally well to this section.

4.1.2.2 User Position Error, Venus Site - Figure 4-18 shows a plot of the horizontal position error at the Venus site. Although the satellite geometry is essentially the same as that for Day 017 (Venus), the horizontal position error plots are notably dissimilar. For example, the initial value of the error shown in Figure 4-9 (Day 017, Venus) is less than 3 meters whereas the corresponding value for Day 029 (Figure 4-18) is 46.3 meters. Moreover, in the case of the Day 017 data, the error returns to the 5 to 20 meter range following the singularity whereas in the case of the Day 029 data it remains above 100 meters.

The individual horizontal error components for Day 029 (Venus) are shown in Figure 4-19. Here again, we note a significant difference in error behavior from that shown in Figure 4-10 for Day 017. In the case of the Day 017 data, the error components are relatively small and somewhat stable before the geometric singularity. This is contrasted with the much larger error excursions shown in Figure 4-19 for Day 029. Of particular note is the large and remarkably linear west-to-east bias trend from -44.0 meters to 55.5 meters in the longitude component for Day 029. Following the geometric singularity, the solution continues to drift east reaching a value of 153.0 meters (east) at the end of the run. As will be seen in the subsequent plots, this general behavior of the solution bias errors is common to the data for the Mojave and Barstow sites. A very substantial effort was made to determine the cause of these bias trends, but the cause remains unknown. It does not appear to involve the

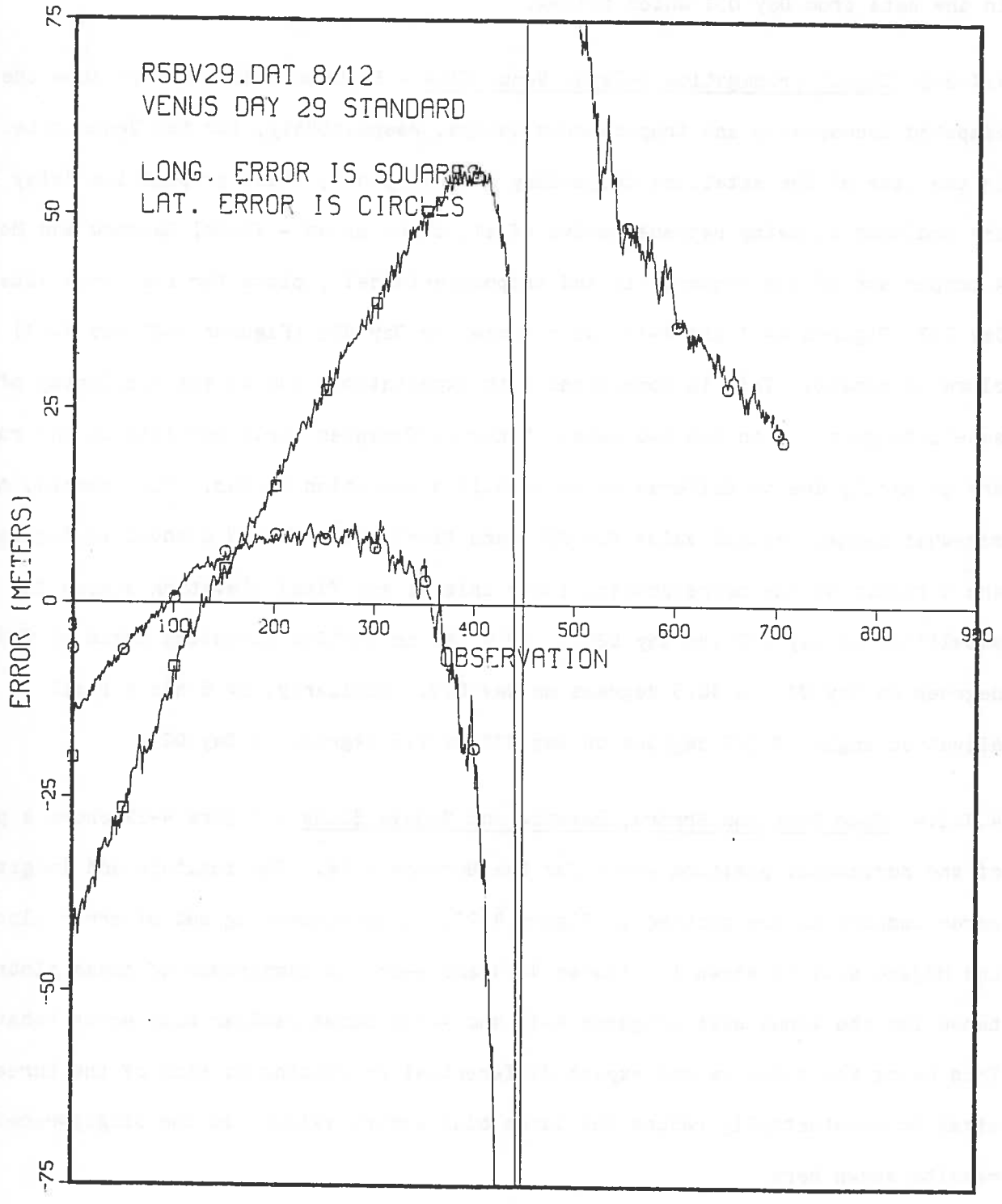

FIGURE 4-19. ERROR COMPONENTS, DAY 029, VENUS SITE

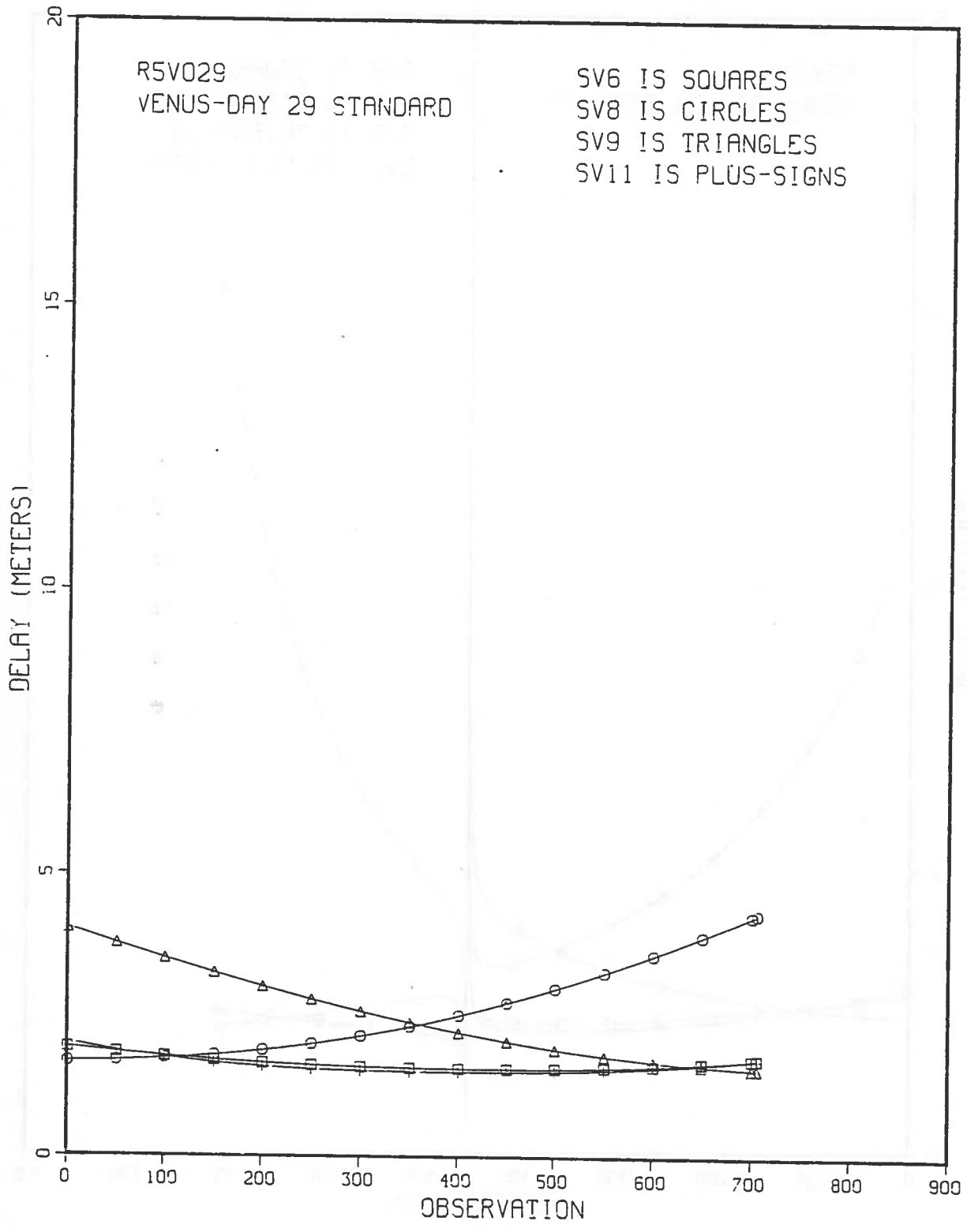

FIGURE 4-20. COMPUTED IONOSPHERIC DELAY, DAY 029, VENUS SITE

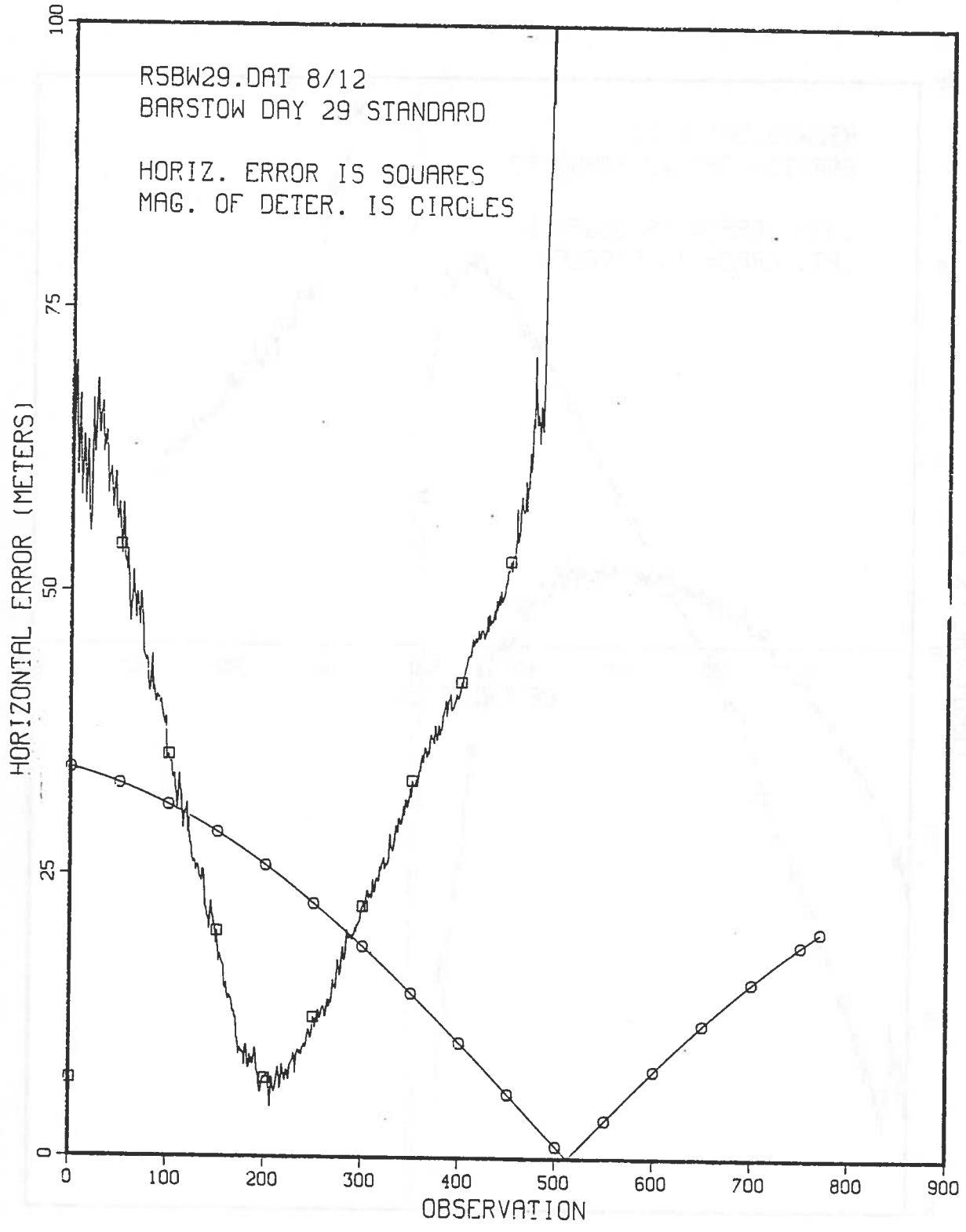

FIGURE 4-22. HORIZONTAL POSITION ERROR, DAY 029, BARSTOW SITE

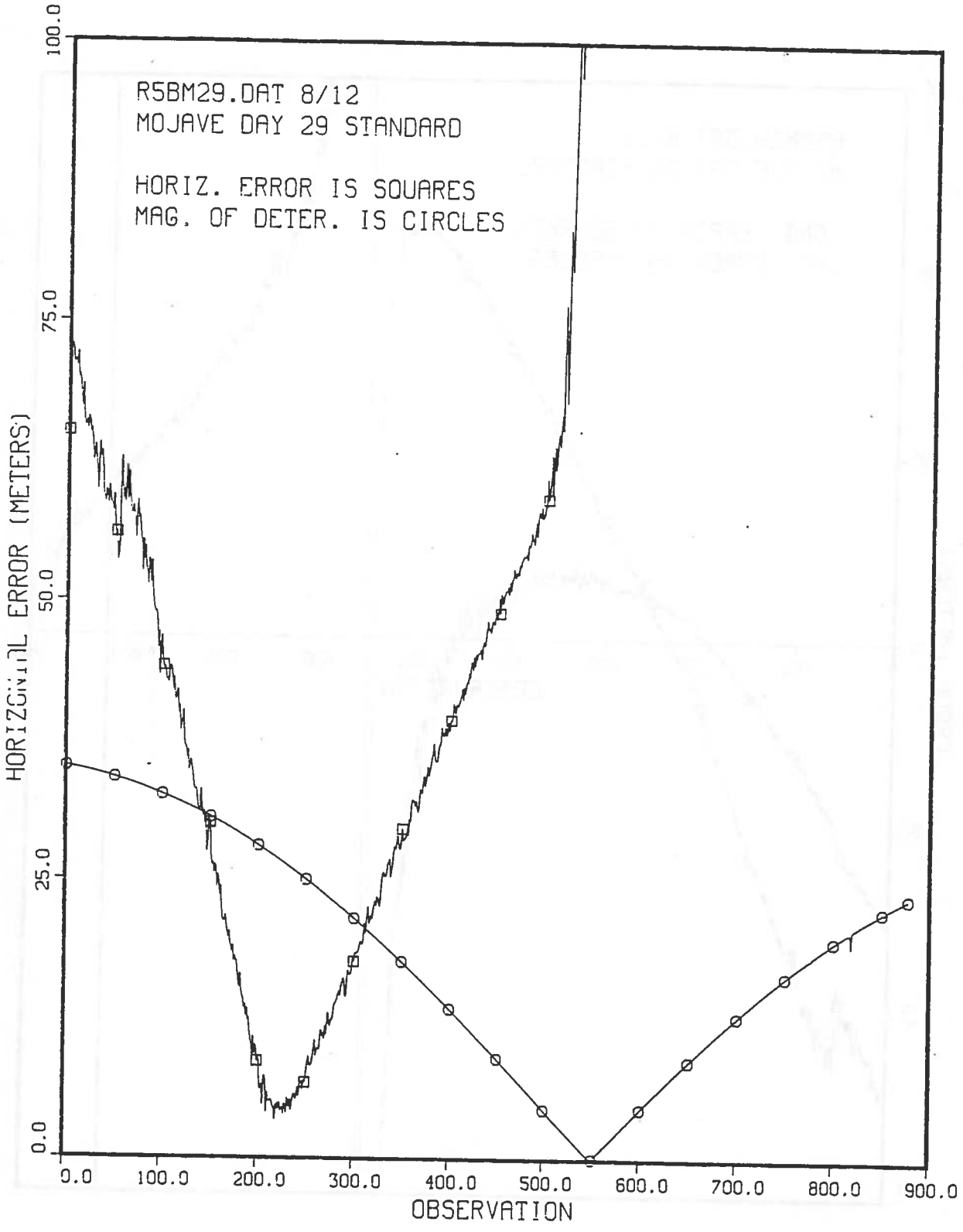

FIGURE 4-24. HORIZONTAL POSITION ERROR, DAY 029, MOJAVE SITE

4.1.2.5 Differential Operation - Data sets from the Venus, Barstow and Mojave site pairs have been processed differentially to remove system bias errors common to all three sites. Data from site pairs are processed by arbitrarily assigning one site to serve as a reference site. The results are shown in Figures 4-26, 4-27 and 4-28. The two longer baselines, Venus/Barstow (22.0 km) and Barstow/Mojave (26.9 km), have differential errors on the order of 5 meters. The shorter baseline, Mojave/Venus (12.7 km), has differential errors on the order of 2 meters. An examination of the differential error component plots (not included) seems to indicate the presence of a residual bias error in longitude associated with the Barstow data. In the case of the Venus/Barstow baseline, there is a nominal 5 meter (east) longitude error. Here, Barstow serves as the reference site. The Barstow/Mojave baseline data contains a nominal -5 meter (west) longitude error. On this baseline, Barstow serves as the remote site. In the case of the Mojave/Venus baseline where the horizontal error is generally 2 meters or less, the latitude and longitude error components show no significant biases.

Although the Barstow data set was the only one to require timetag/pseudorange correction (-0.625 milliseconds), this fact is probably of no significance. Both the Venus and Harvard site data required much larger timetag/pseudorange corrections (23.0 milliseconds and 8.35 milliseconds, respectively) on Day 017. In the case of Day 017, there were no significant bias errors in the differential error components over a very much longer baseline of 1,302.3 kilometers.

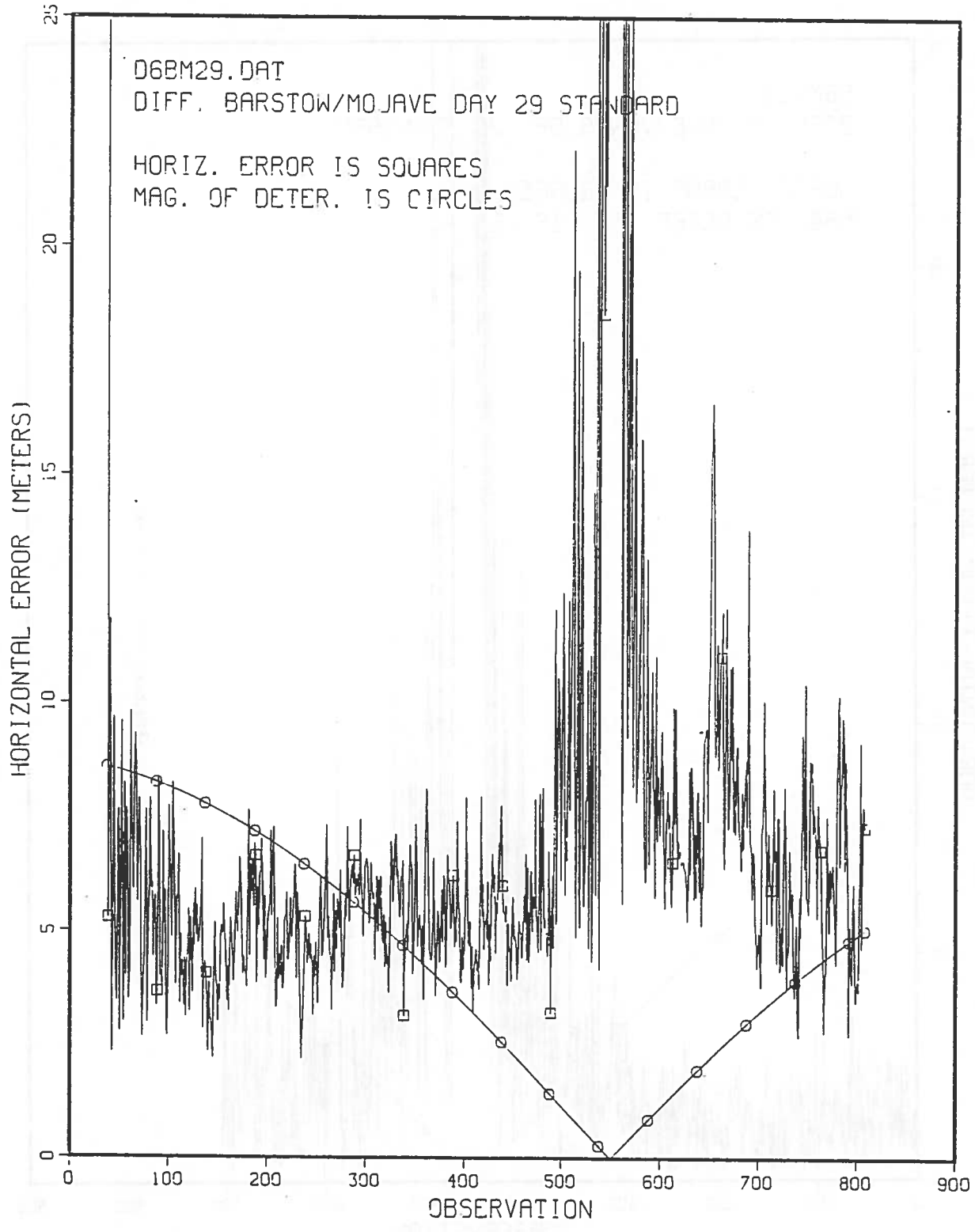

FIGURE 4-27. HORIZONTAL DIFFERENTIAL ERROR, DAY 029, BARSTOW/MOJAVE BASELINE

4.1.3 Day 031, Venus/Point Sites

The Point VLBI site serves as the reference site in this two-receiver test. The Venus/Point baseline of 91.7 kilometers is of intermediate length as compared to the Day 017 Venus/Harvard baseline (1302.3 kilometers) and those of Day 029 which range from 2.7 to 26.9 kilometers. Geodetic and WGS-72 coordinates of the marks are:

Venus (site number 85031)

Latitude: 35 degrees, 14 minutes, 53.11116 seconds

Longitude: 243 degrees, 12 minutes, 27.35881 seconds

Height: 1.037937 kilometers above ref. ellipsoid

X = -2350.906034 kilometers

Y = -4655.537189 kilometers

Z = 3660.976579 kilometers

The offsets of the phase center of the antenna from the mark are:

0.000 meters north

0.000 meters east

1.042 meters above ref. ellipsoid

Point (site number 85039)

Latitude: 34 degrees, 27 minutes, 13.60196 seconds

Longitude: 242 degrees, 55 minutes, 55.11976 seconds

Height: 0.90520 kilometers above ref. ellipsoid

X = -2396.141915 kilometers

Y = -4688.923195 kilometers

Z = 3588.576305 kilometers

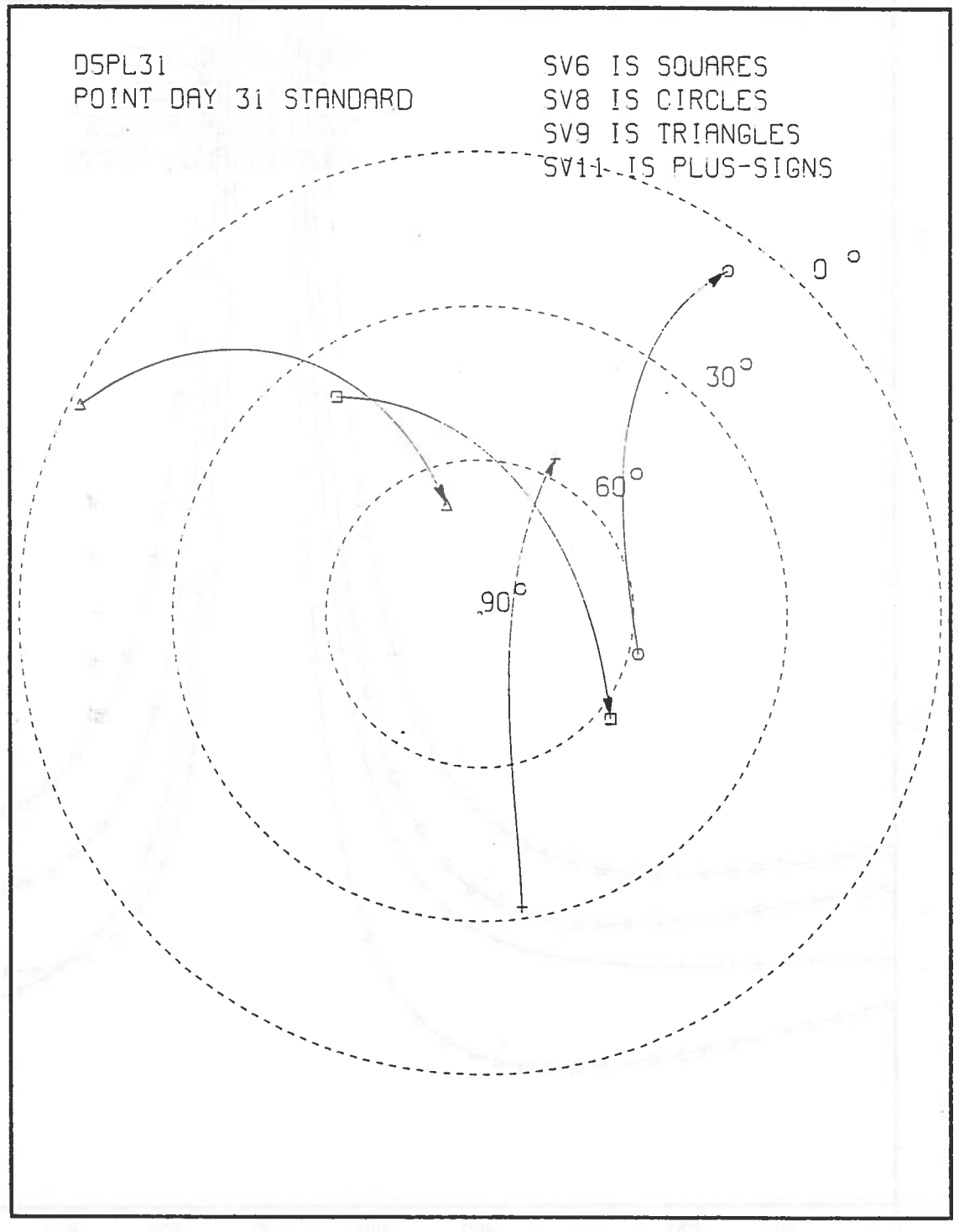

FIGURE 4-29. SATELLITE GEOMETRY, DAY 031, POINT SITE

4.1.3.2 User Position Error, Point Site - Figure 4-31 shows a plot of the horizontal position error for the Point site. Horizontal position error is on the order of 12 meters before the geometric singularity, reaching 20.8 meters at observation number 511 where HDOP has risen to 6.0. Following the singularity, HDOP falls to below 6.0 (at observation number 731) and horizontal position error remains in the 12 to 25 meter range. The discontinuity in the error plot at observation number 150 is of unknown origin. It may be associated with a satellite upload since the log for the Yuma test range shows an upload of SVs 9 and 11 approximately 30 minutes later. Unfortunately, the Yuma log does not begin until after the time of the discontinuity. Since data recording at the Venus site does not begin until observation number 191, the discontinuity occurs outside of the time span of differential processing. The corresponding error components are shown in Figure 4-32.

4.1.3.3 Signal Propagation Delay, Point Site - Figures 4-33 and 4-34 show the computed ionospheric and tropospheric delays respectively for the Point site. Due to the proximity of the Venus site, the plots shown are also considered to be representative of the Venus site. The computed ionospheric delays shown in Figure 4-33 are essentially identical to those computed for the Venus site (not shown) and are quite similar to those shown in Figure 4-20 for the Venus site on Day 029. Since the data collection interval is during the nighttime hours, the delay simply follows the obliquity factor. The computed tropospheric delay shown in Figure 4-34 (Point, Day 031), contains an unusually large delay for SV 9 at the start of the run. This is due to the very low elevation angle of SV 9 which begins the run at an elevation angle of only 1.4 degrees. When SV 9 reaches an elevation angle of 10.5 degrees (its initial elevation angle on Day 029 as seen from the Venus site), the delay is essentially the same as shown in Figure 4-21.

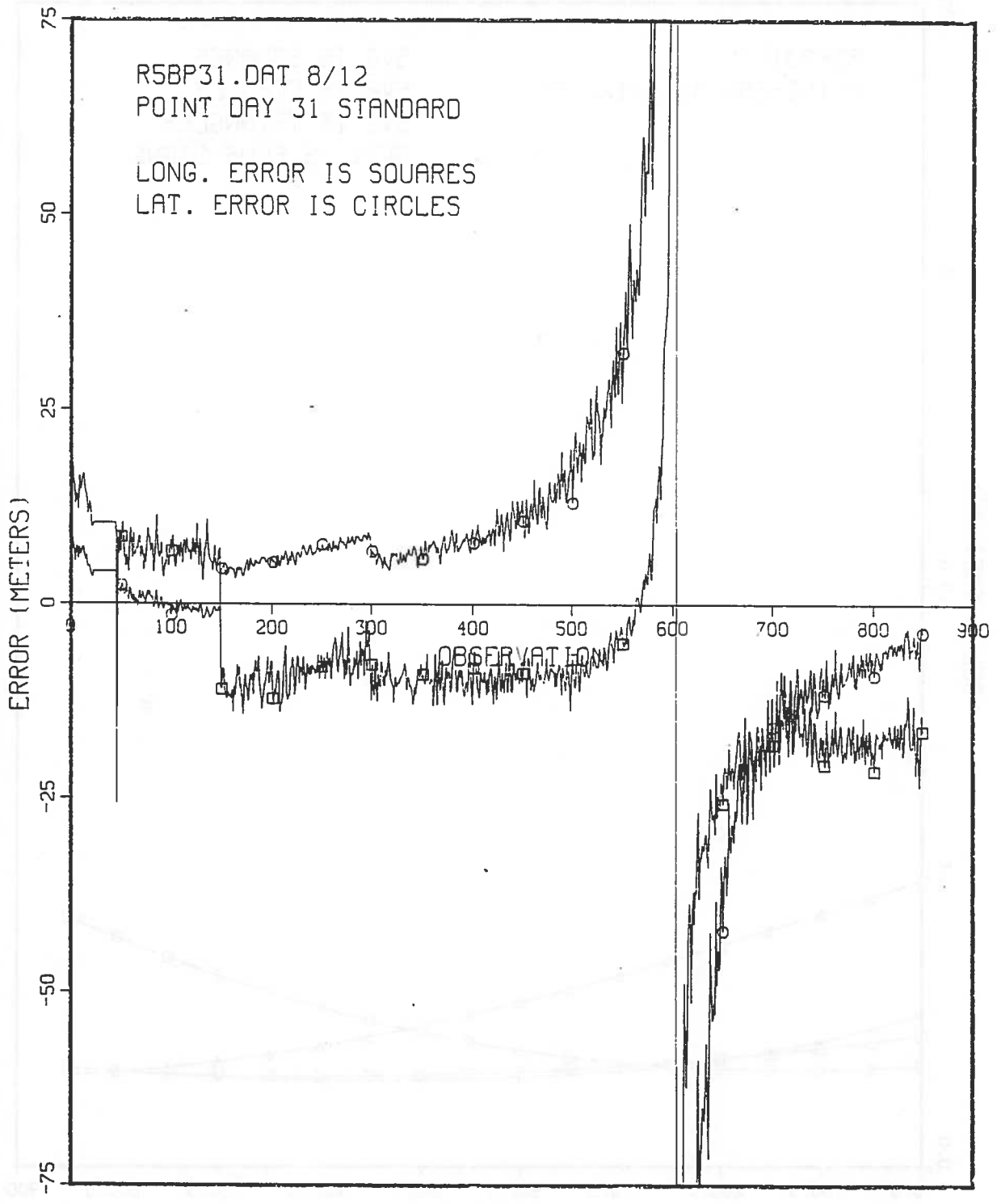

FIGURE 4-32. ERROR COMPONENTS, DAY 031, POINT SITE

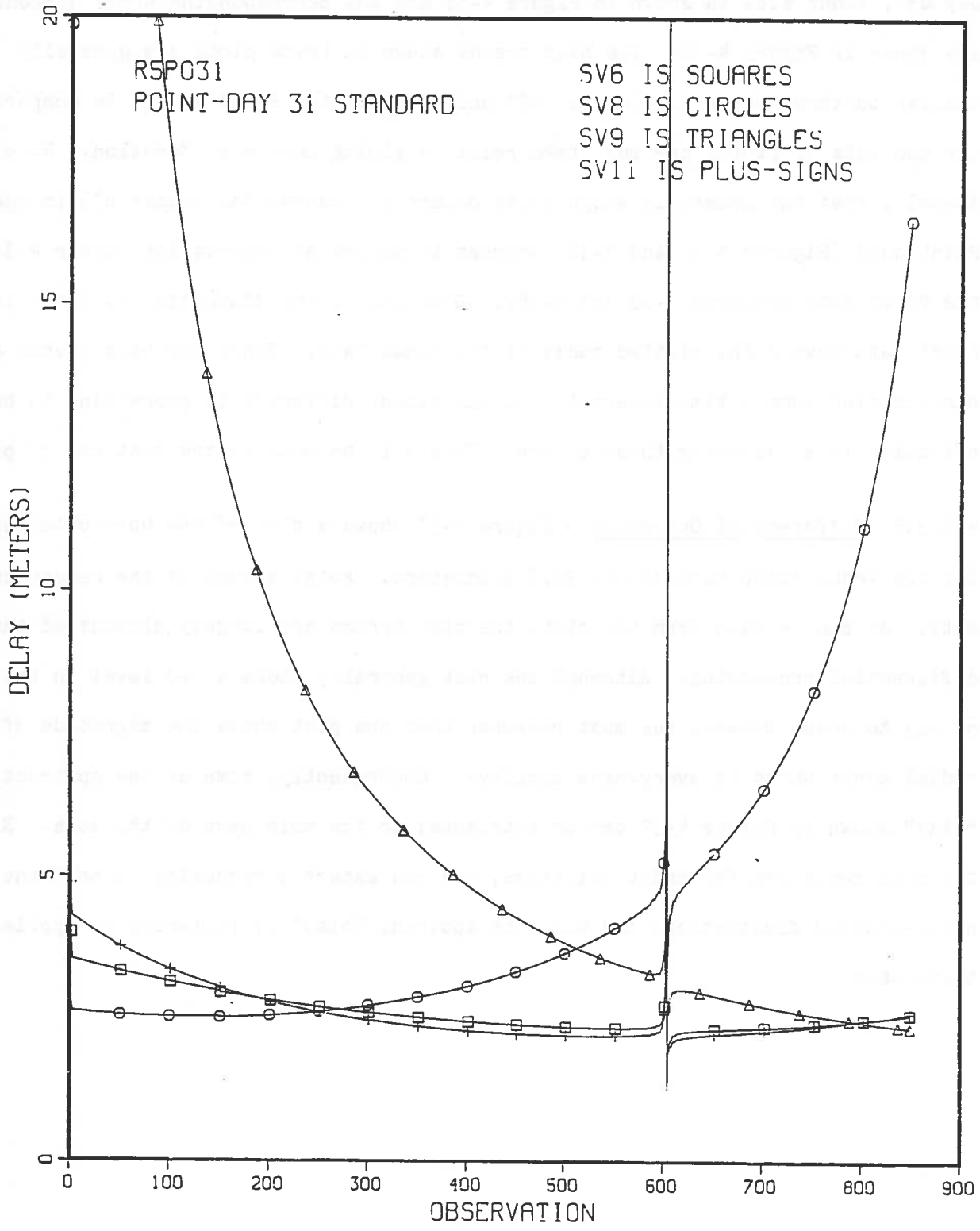

FIGURE 4-34. COMPUTED TROPOSPHERIC DELAY, DAY 031, POINT SITE

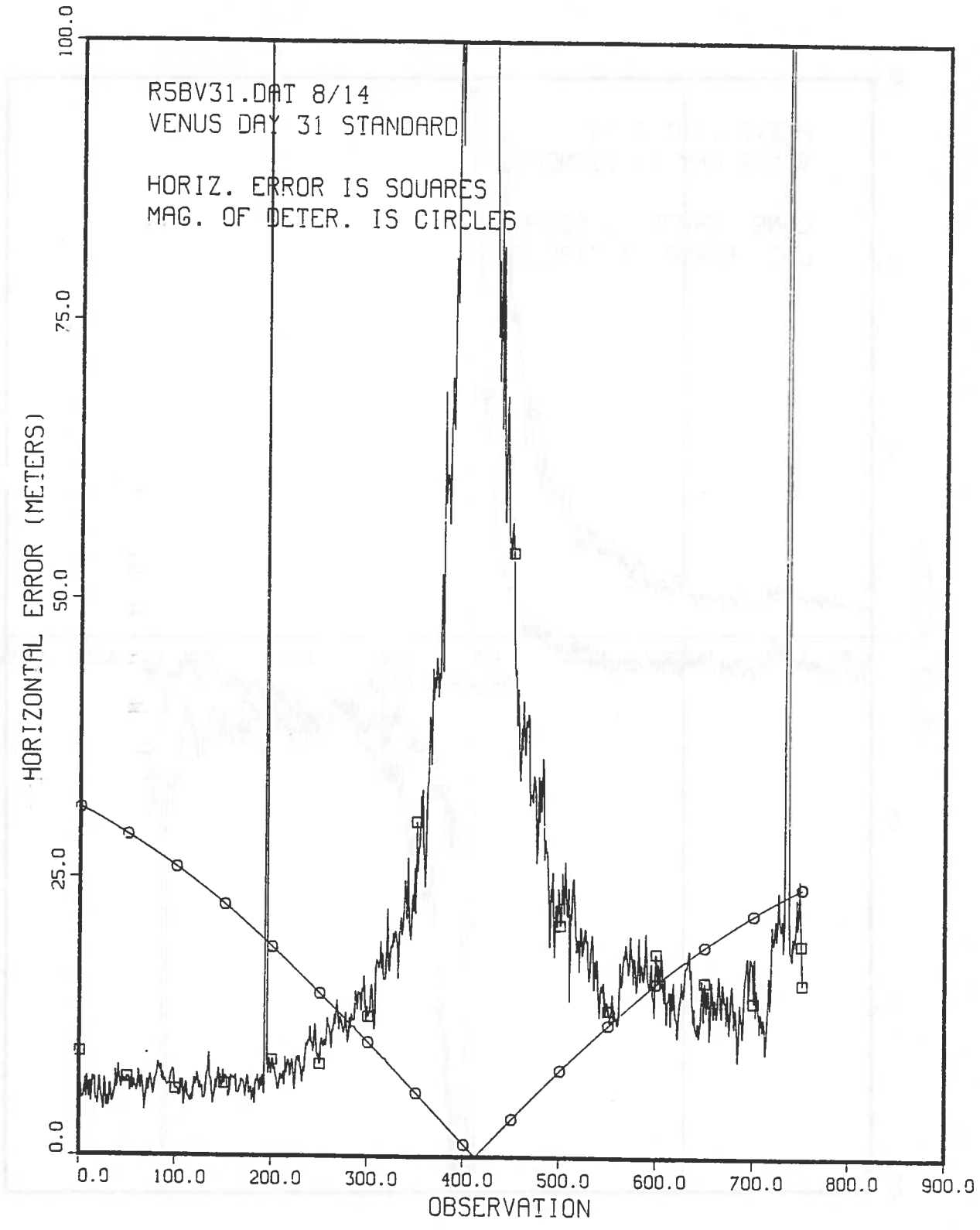

FIGURE 4-35. HORIZONTAL POSITION ERROR, DAY 031, VENUS SITE

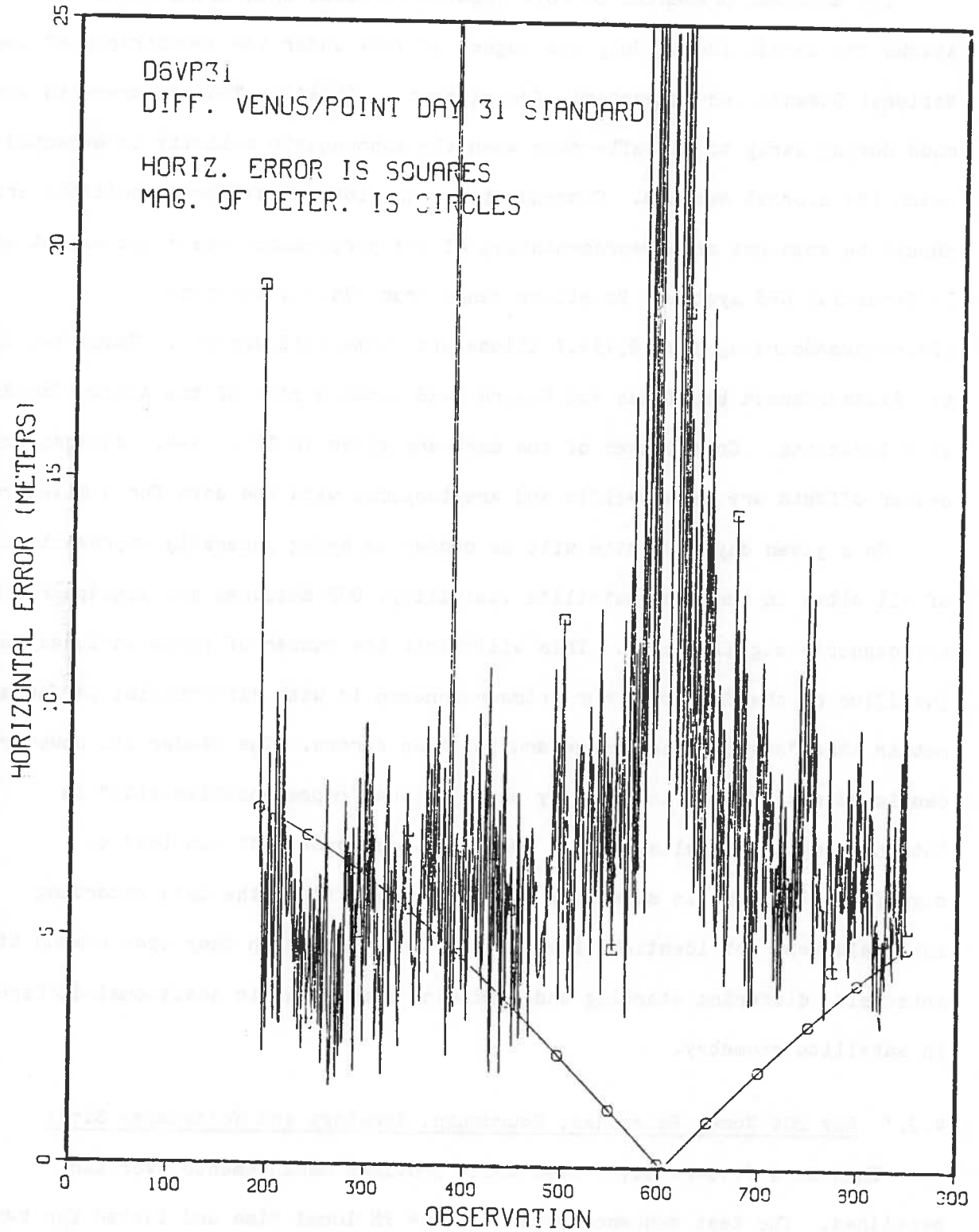

FIGURE 4-37. HORIZONTAL DIFFERENTIAL ERROR, DAY 031, VENUS/POINT BASELINE

TABLE 4-3. ALASKA/CANADA SITE BASELINES

(kilometers)

DAY 208

NOME/FAIRBANKS	848.4
NOME/SOURDOUGH	1,003.6
NOME/YAKATAGA	1,276.2
NOME/WHITEHORSE	1,591.1
FAIRBANKS/SOURDOUGH	276.3
FAIRBANKS/YAKATAGA	603.0
FAIRBANKS/WHITEHORSE	788.8
SOURDOUGH/YAKATAGA	329.3
SOURDOUGH/WHITEHORSE	591.3
YAKATAGA/WHITEHORSE	414.2

DAY 213

NOME/FAIRBANKS	848.4
NOME/YELLOWKNIFE	2,459.7
FAIRBANKS/YELLOWKNIFE	1,631.1

DAY 219

NOME/FAIRBANKS	848.4
NOME/SAND POINT	1,060.0
FAIRBANKS/SAND POINT	1,284.6

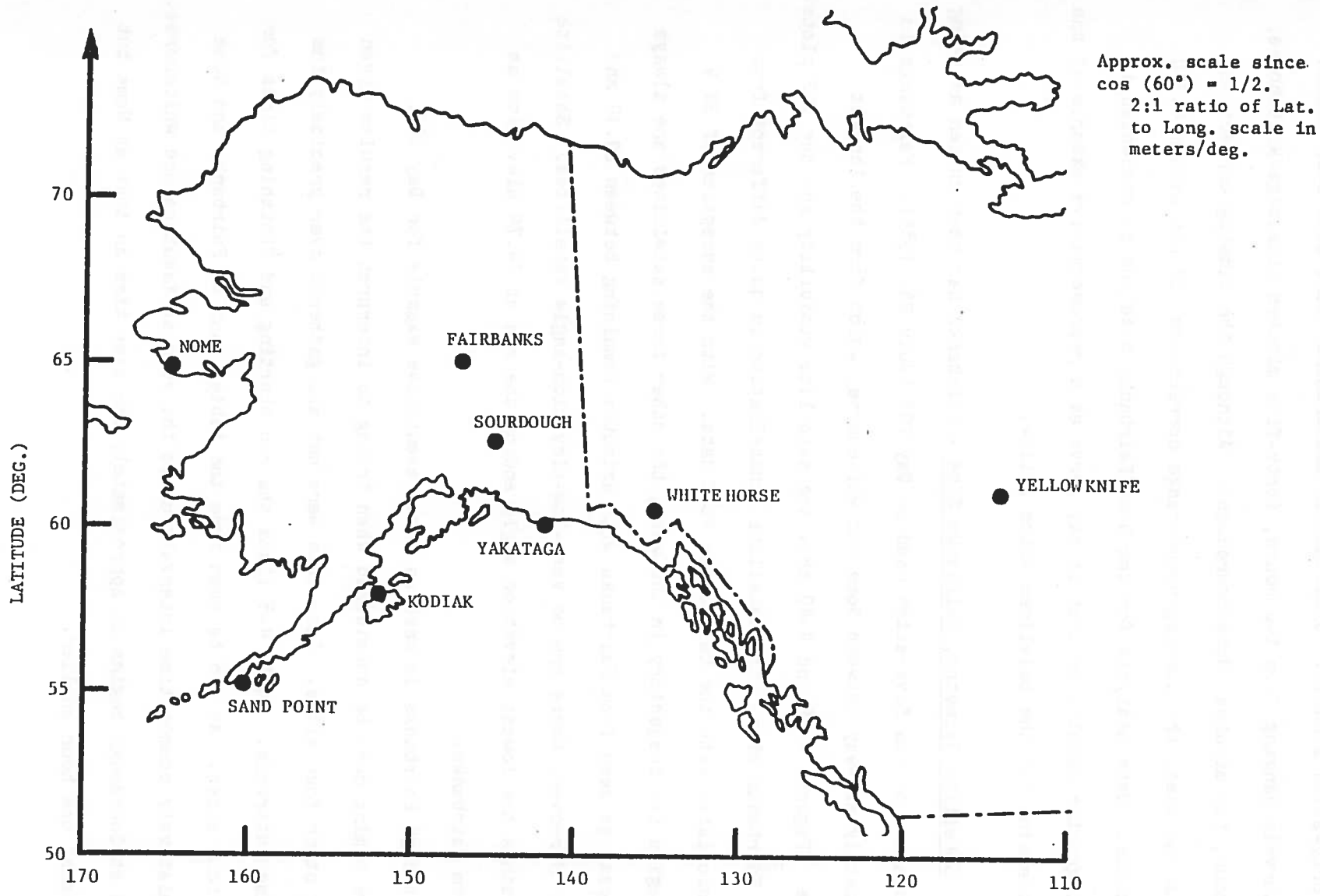

FIGURE 4-38. ALASKA/CANADA SITE LOCATIONS

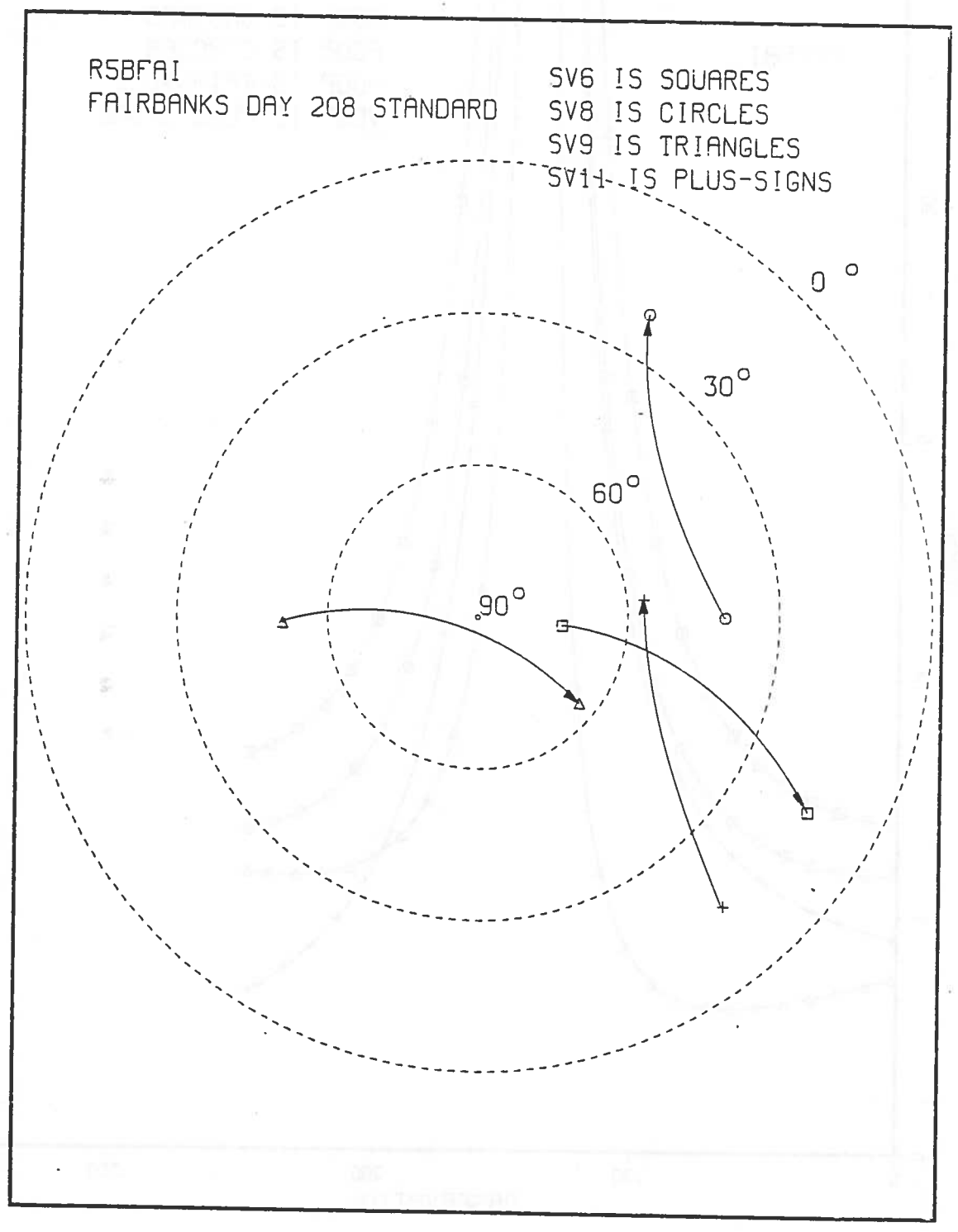

FIGURE 4-39. SATELLITE GEOMETRY, DAY 208, FAIRBANKS

4.2.1.2 User Position Error, Fairbanks Site - Figure 4-41 shows a plot of the horizontal position error at the Fairbanks site. The error remains relatively constant, averaging approximately 14 meters during the first 100 observations for which HDOP is less than 4.1. Thereafter, the horizontal position error increases rapidly, reaching 19.2 meters at observation number 112 where HDOP has increased to 5.9. Following the geometric singularity at observation number 139, HDOP falls below 6.0 at observation number 207 and remains between 6.0 and 5.9 for the remainder of the run. The horizontal position error is relatively constant, averaging about 9 meters, during this last portion of the run. Individual error components are plotted in Figure 4-42.

4.2.1.3 Signal Propagation Delays, Fairbanks Site - The computed ionospheric delays for the Fairbanks site are shown in Figure 4-43. Upon initial observation, one might conclude that the ionospheric delays shown are lower than what might, at first, be expected based upon the California VLBI nighttime data. For example, the plot shown in Figure 4-5 for the Harvard site is remarkably similar. Two factors account for the apparently lower than expected ionospheric delays. Plots given by Klobuchar (3) show a general decline in the magnitude of the amplitude term with increasing latitude. Moreover, the plots also show a seasonal decline in the magnitude of the amplitude term going from winter to summer. Using relatively approximate scaling methods we find that the curves given in reference (3) indicate a 2.2 meter ionospheric delay versus the 1.37 meters shown for SV 9 at observation number 150 in Figure 4-43. This is reasonable agreement.

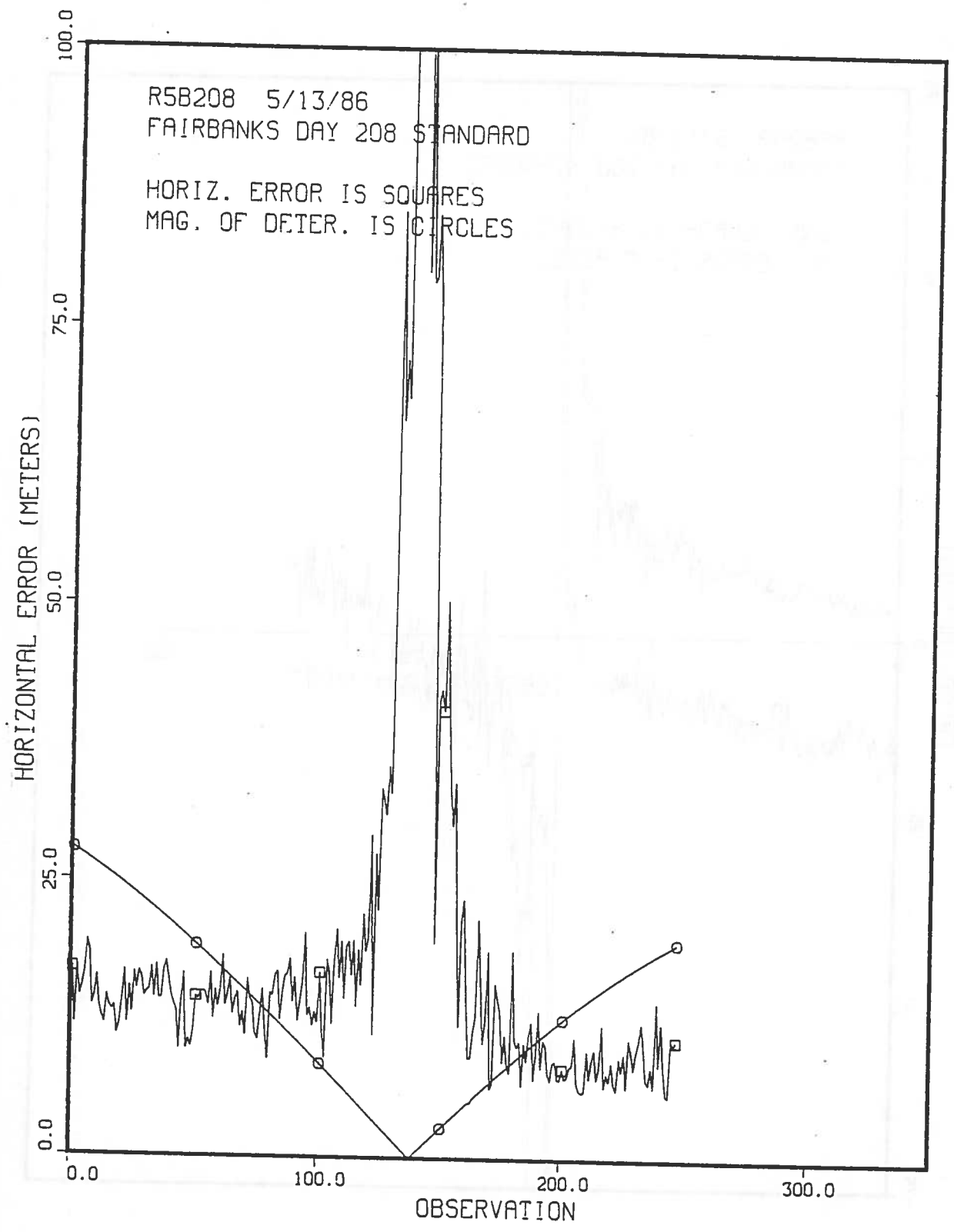

FIGURE 4-41. HORIZONTAL POSITION ERROR, DAY 208, FAIRBANKS

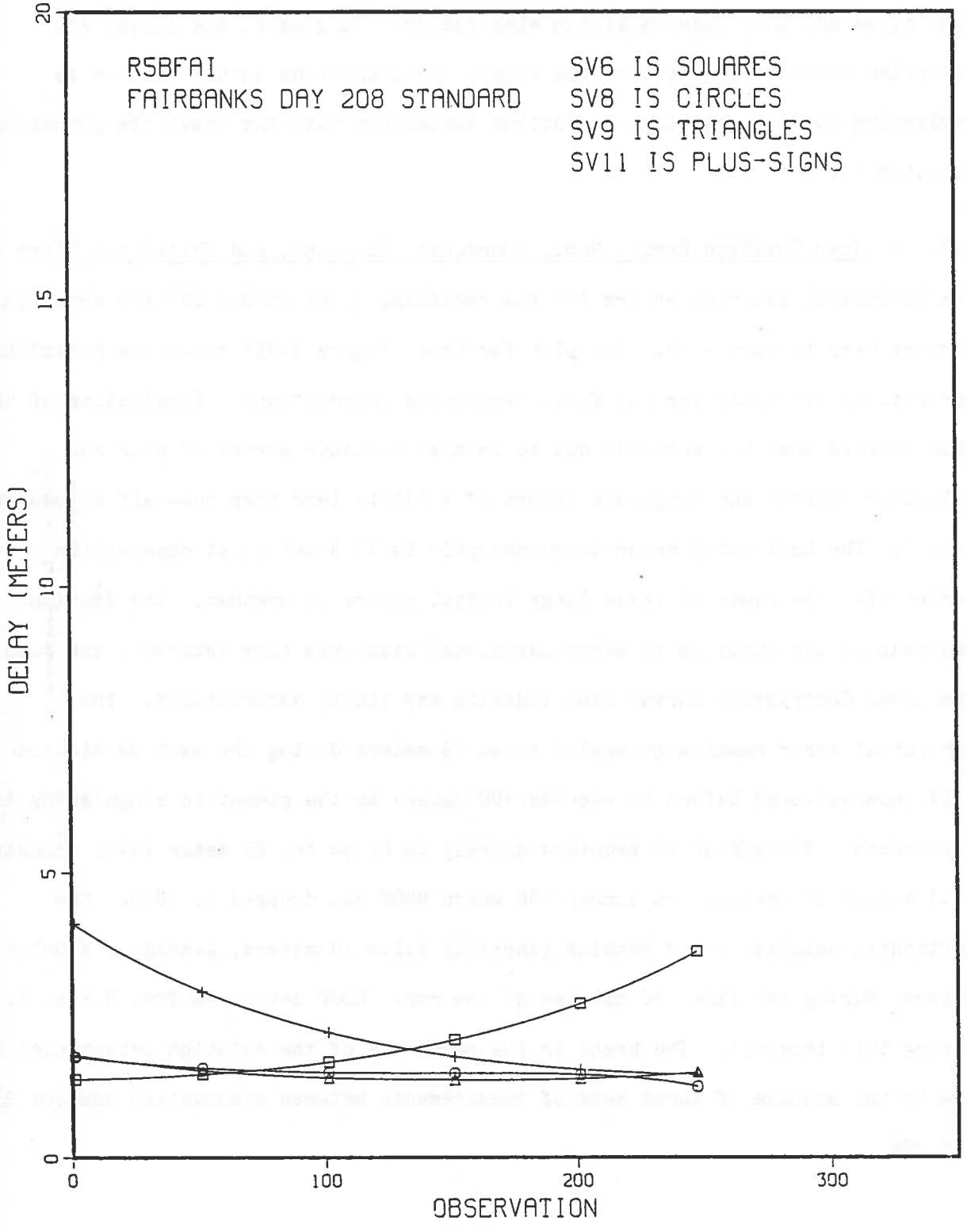

FIGURE 4-43. COMPUTED IONOSPHERIC DELAY, DAY 208, FAIRBANKS

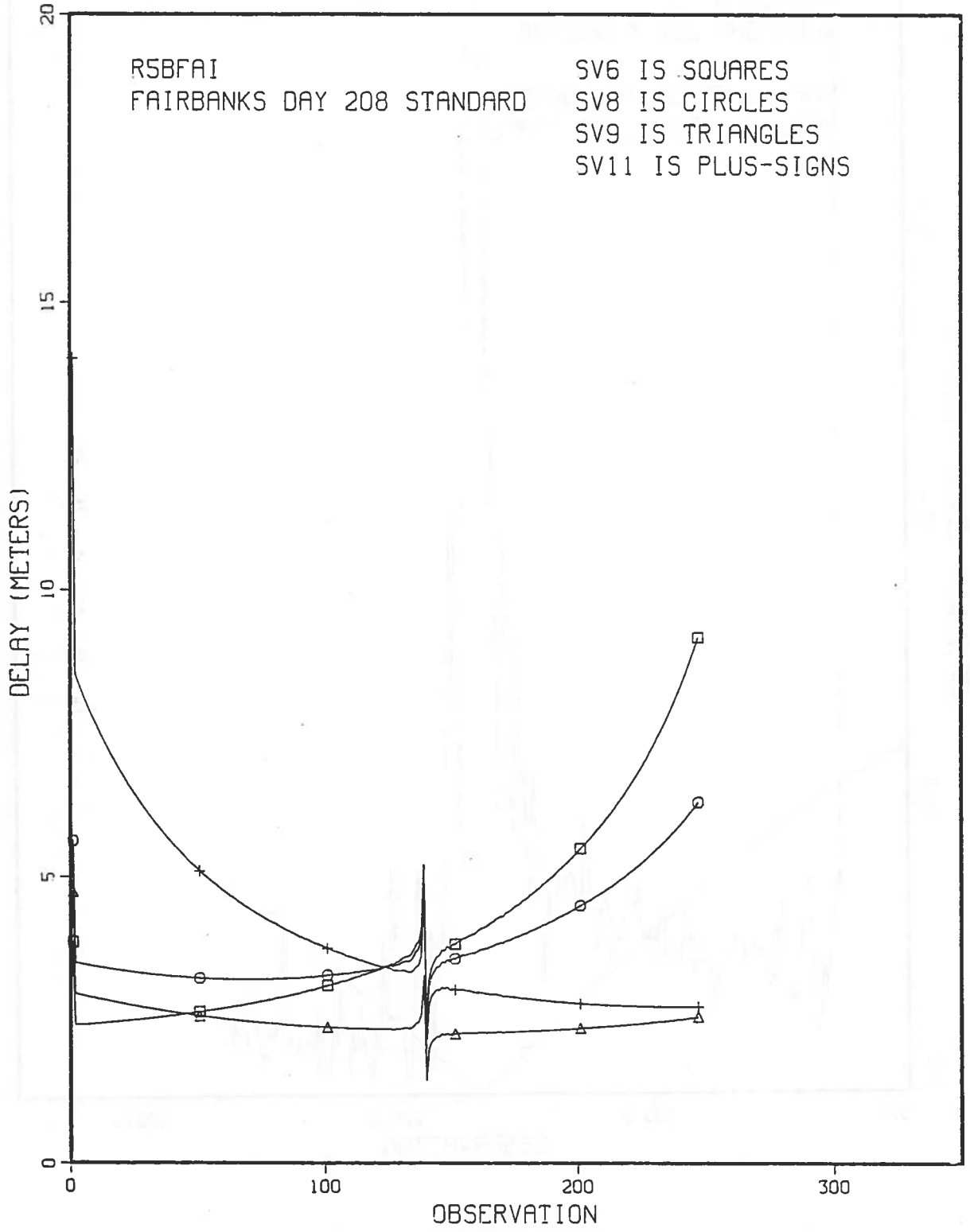

FIGURE 4-44. COMPUTED TROPOSPHERIC DELAY, DAY 208, FAIRBANKS

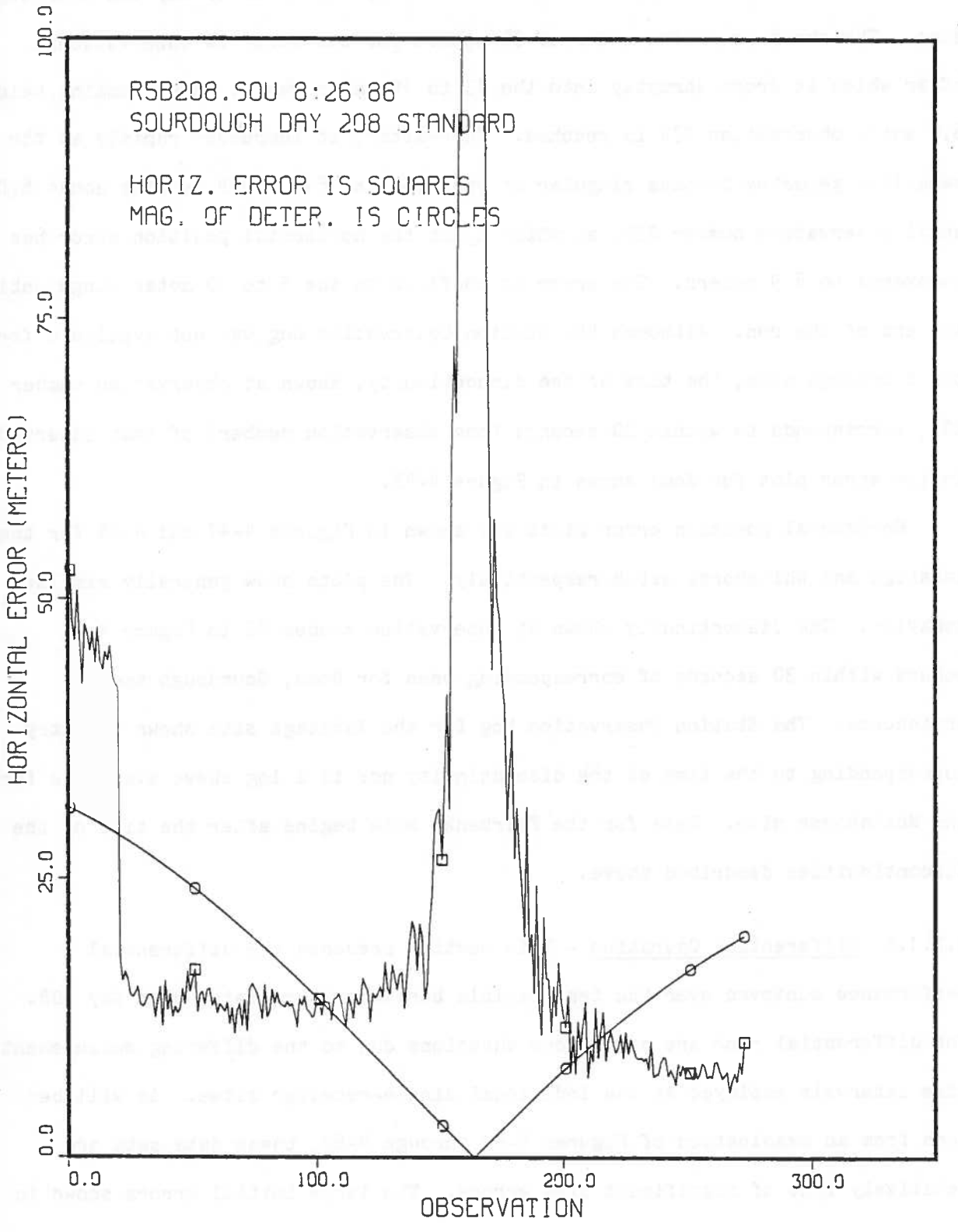

FIGURE 4-46. HORIZONTAL POSITION ERROR, DAY 208, SOURDOUGH

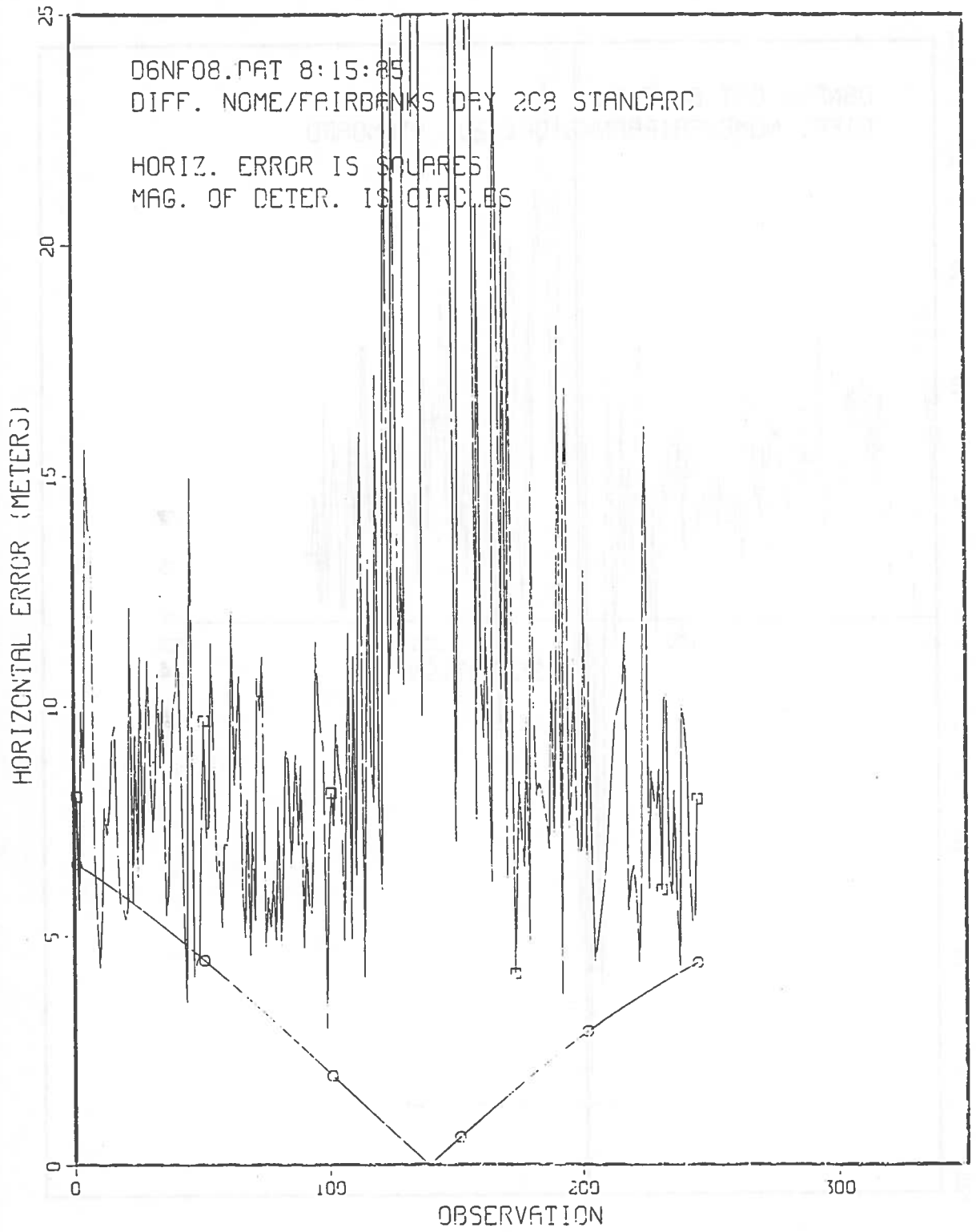

FIGURE 4-49. HORIZONTAL DIFFERENTIAL ERROR, DAY 208, NOME/FAIRBANKS BASELINE

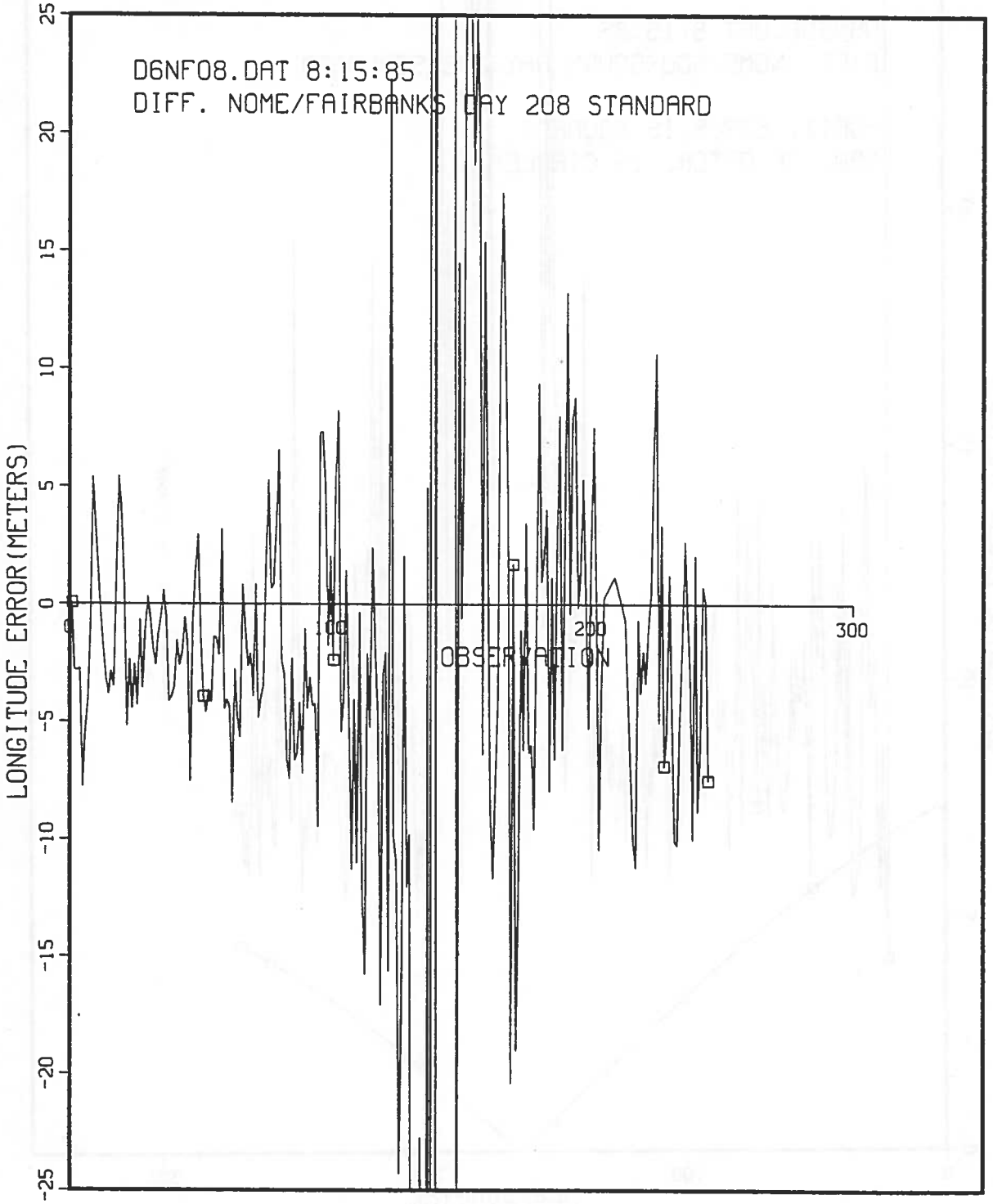

FIGURE 4-51. DIFFERENTIAL ERROR, LONGITUDE COMPONENT, DAY 208, NOME/FAIRBANKS BASELINE

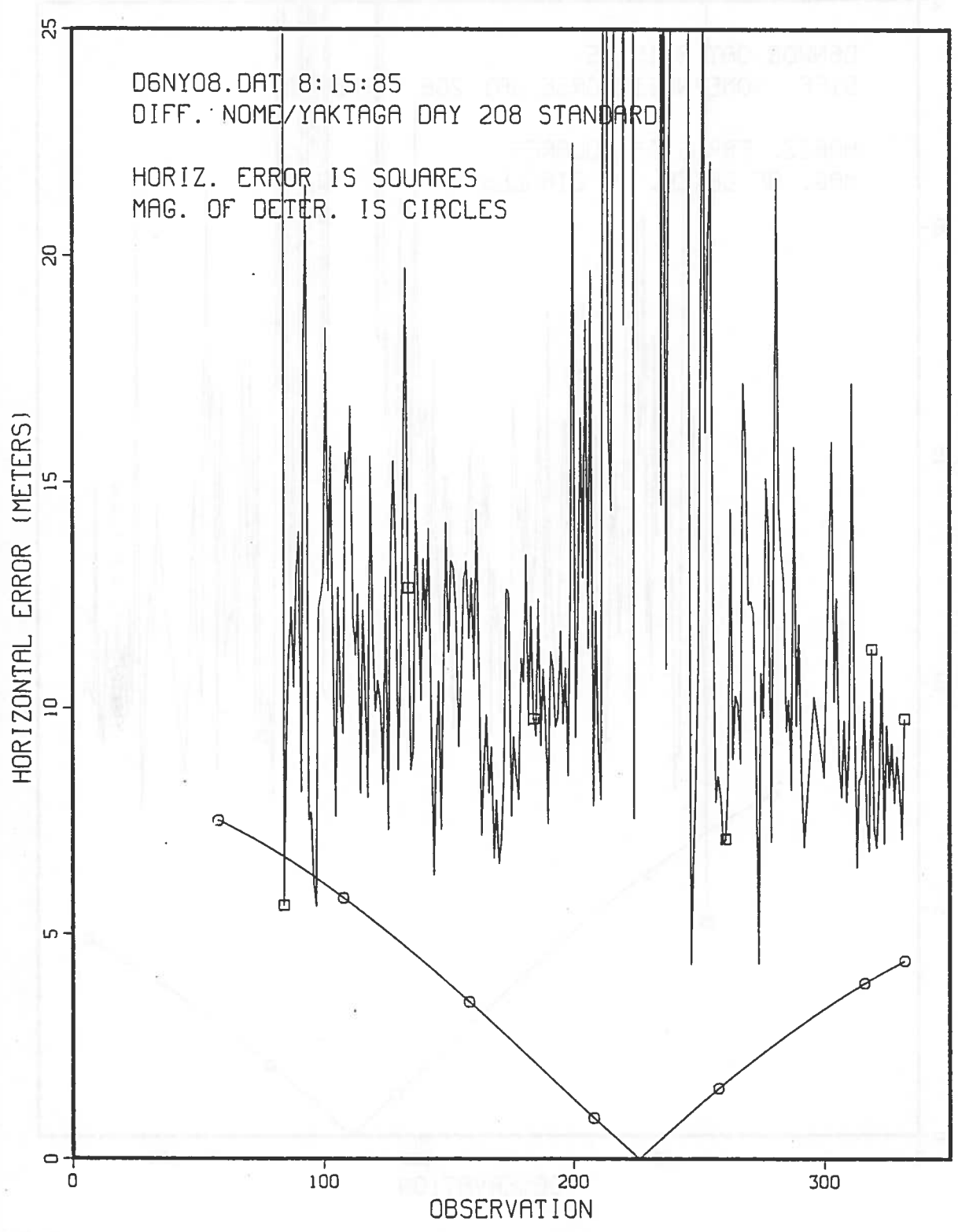

FIGURE 4-53. HORIZONTAL DIFFERENTIAL ERROR, DAY 208, NOME/YAKATAGA BASELINE

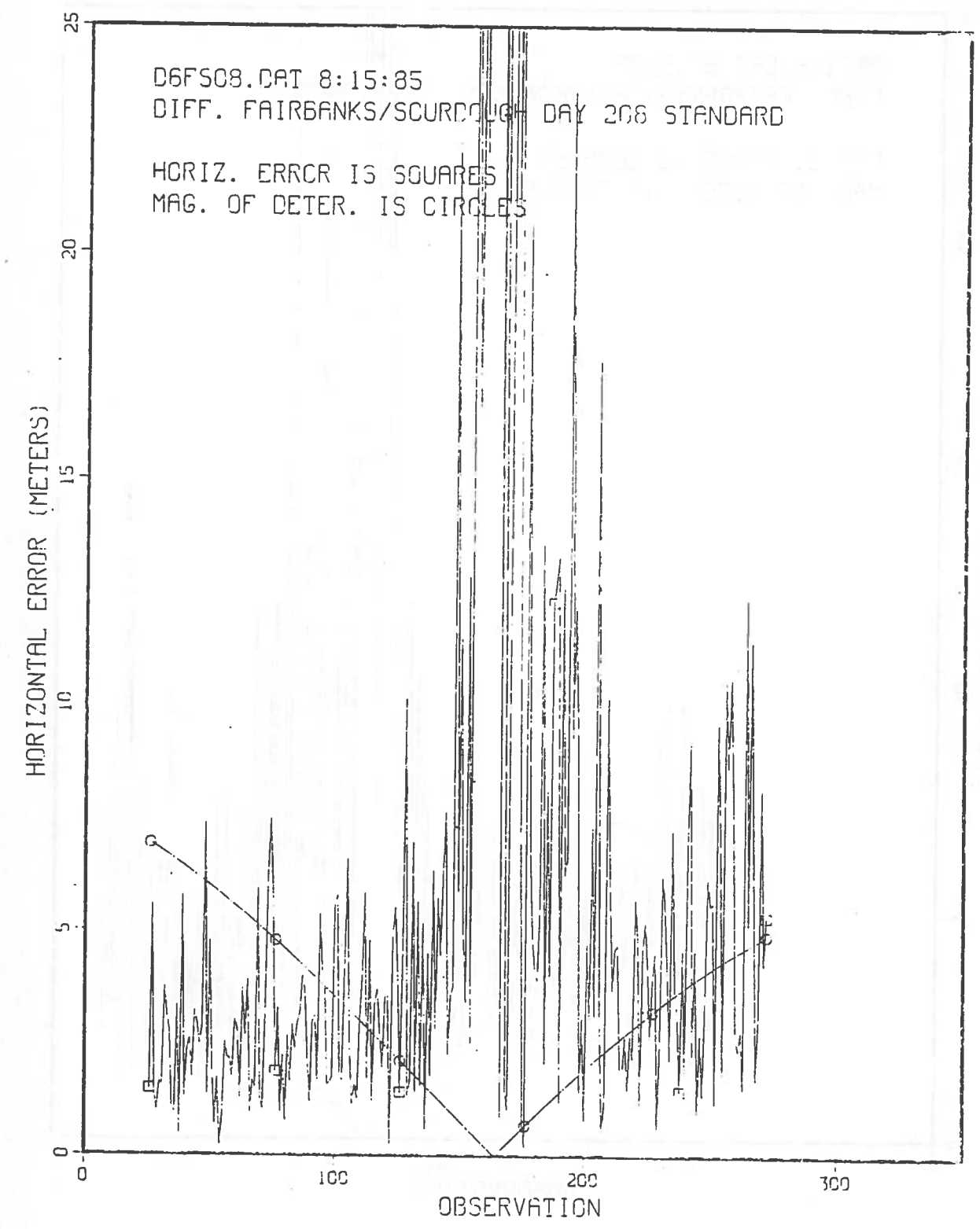

FIGURE 4-55. HORIZONTAL DIFFERENTIAL ERROR, DAY 208, FAIRBANKS/SOURDOUGH BASELINE

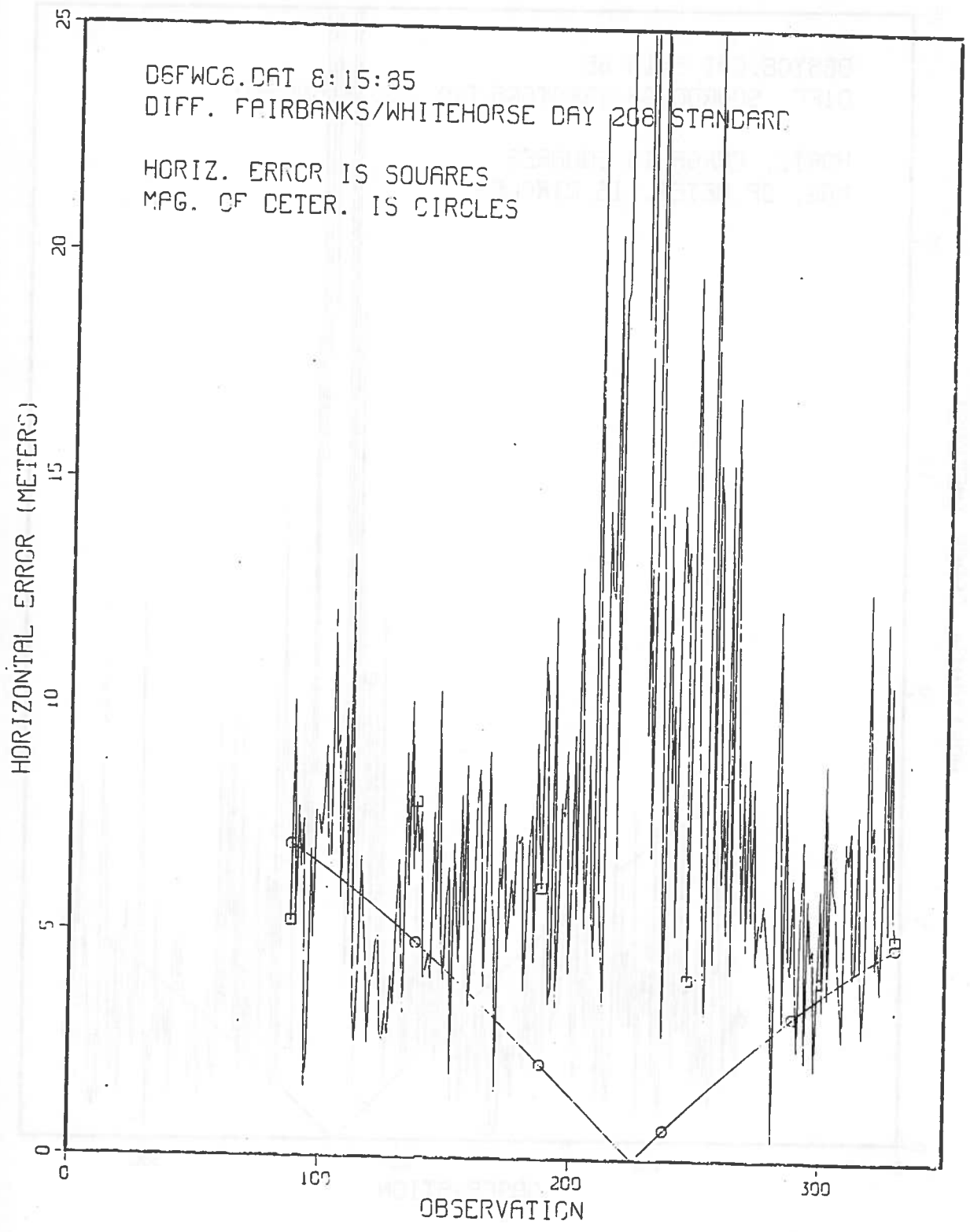

GURE 4-57. HORIZONTAL DIFFERENTIAL ERROR, DAY 208, FAIRBANKS/WHITEHORSE BASELINE

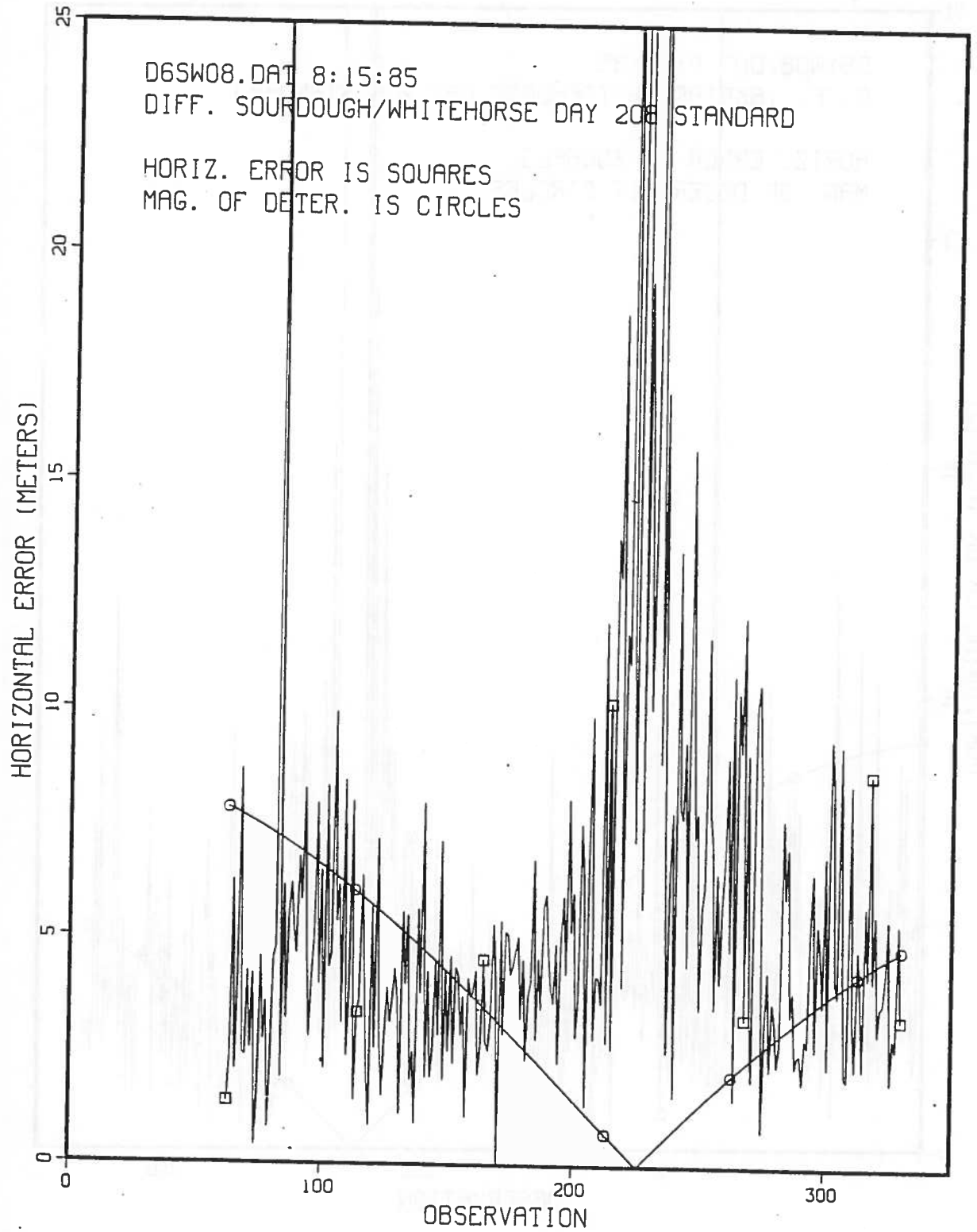

FIGURE 4-59. HORIZONTAL DIFFERENTIAL ERROR, DAY 208, SOUDOUGH/WHITEHORSE BASELINE

Figures 4-52, 4-53 and 4-54 are due to an apparent problem with the Nome data at the beginning of the run (see Figure 4-45). During the first thirteen minutes of the Nome data recording interval, the horizontal position error was in excess of one kilometer.

Differential error statistics were computed for those regions over which HDOP remained less than or equal to 6.0. This prevents the very large errors associated with the singularity in satellite geometry from unduly influencing the statistics. Moreover, when the full satellite constellation becomes available, HDOP will generally remain below 6.0. Linear regression lines (least squares fit) were computed for each of the error statistics. These, along with the associated correlation coefficient, are included on the plots which follow.

If we neglect those portions of the differential runs which are influenced by the geometric singularity, we find that the horizontal differential position error average is between 3.10 and 13.18 meters. The corresponding latitude and longitude error components fall between 1.41 and 12.08 meters and -4.43 and 1.60 meters respectively.

A plot of the mean horizontal error values as a function of baseline length is given in Figure 4-61. The relationship shown is remarkably linear, evidencing a slope of approximately 8.2 meters per one thousand kilometers for baselines of 276.3 to 1591.1 kilometers. The correlation for the data shown is 0.985. For baselines between 200 and 600 kilometers, the slope is approximately 3.3 meters per one thousand kilometers starting from an initial offset of approximately 2.9 meters at 200 kilometers. A similar plot of the mean differential latitude error components is given in Figure 4-62. The latitude error component shows a slope of approximately 8.9 meters (north) per one thousand kilometers. The corresponding correlation coefficient is 0.988. The

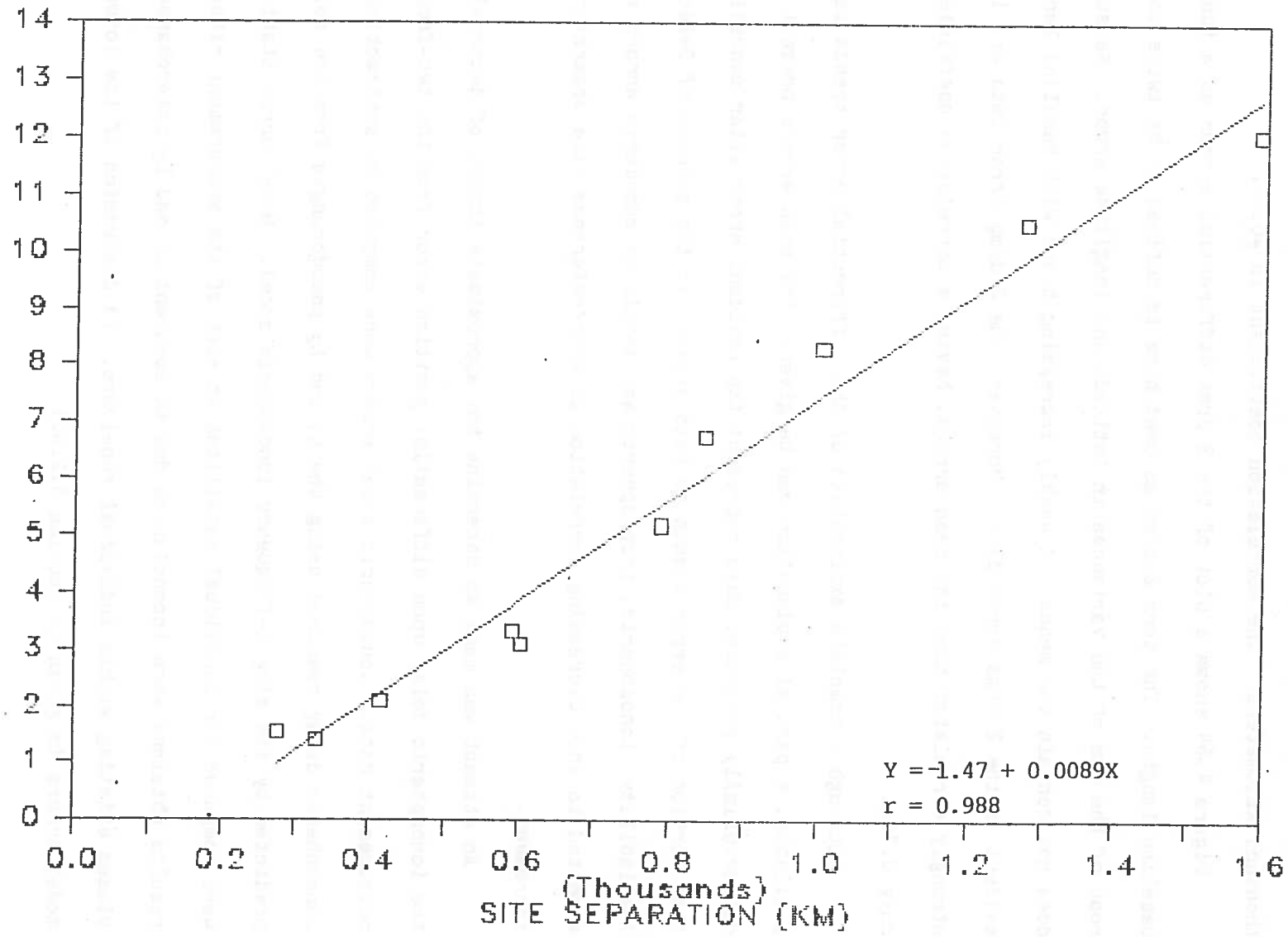

FIGURE 4-62. MEAN DIFFERENTIAL LATITUDE ERROR VS BASELINE LENGTH, DAY 208, HDOP $\leq$ 6.0

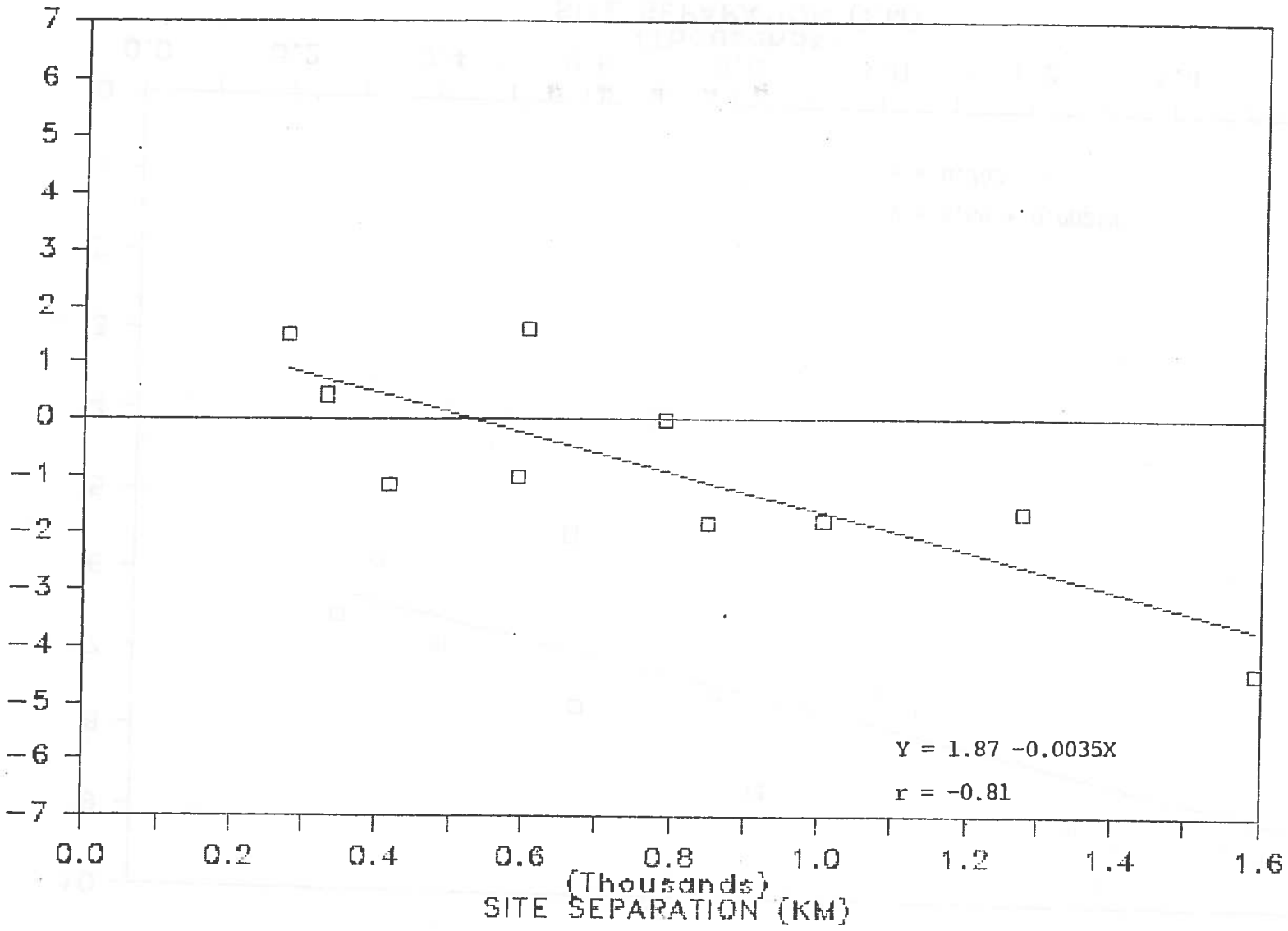

FIGURE 4-63. MEAN DIFFERENTIAL LONGITUDE ERROR VS BASELINE LENGTH, DAY 208, HDOP≤6.0

Satellite broadcast ephemeris errors constitute a second component of the mean differential errors. Again, the Nome/Sourdough baseline was chosen in an attempt to explain the error trends observed. Precise ephemeris data were obtained and a comparison made between the satellite position determined from the broadcast ephermeris and the precise ephemeris. This was done for each satellite at a time corresponding to observation number 177 in the Nome Day 208 data. The ephemeris differences were found to be 26.72 meters, 5.94 meters, 8.39 meters and 19.26 meters for SVs 6, 8, 9 and 11 respectively. If these errors are taken to be along-track errors (worst case), they translate into pseudorange differences of 1.34 meters, 0.30 meters, 0.42 meters and 0.96 meters respectively over a 1,003.6 kilometer baseline. Since the signs of the pseudorange differences were unknown, a crude approximation of their possible impact was determined by assuming a single 1.25 meter pseudorange difference and applying it successively to each of the four pseudoranges. Multiplication by the solution matrix for Nome gave horizontal position increments of 2.9 meters, 3.3 meters, 1.6 meters and 1.7 meters for SV 6, 8, 9 and 11 pseudoranges respectively. These values range from 18 percent to 37 percent of the mean horizontal differential error of 8.99 meters found for the Nome/Sourdough baseline. Although the approximations used are admittedly crude, the results obtained are not inconsistent with the results obtained on this baseline. Moreover, an examination of the relationship between baseline length and pseudorange differences shows the relationship to be linear over baselines up to 2,000 kilometers and more.

The above observations tend to support the validity of the differential error trends observed in the Day 208 data. Additional contributions from the troposphere and receiver measurement noise can be expected to account for an

4.2.2 Day 213, Nome, Fairbanks and Yellowknife Sites

Data were taken at three sites and processed differentially over three baselines. Two of those baselines evidenced unusually large differential errors which may have resulted from questionable measurement data at the Nome site. The mean horizontal differential error (HDOP $\leq$ 6.0) for the Nome/Fairbanks baseline of 848.4 kilometers was 48.07 meters while the corresponding error for the 2495.7 kilometer Nome/Yellowknife baseline was 29.78 meters. Neither of these data sets is thought to be valid and both have been eliminated from further consideration. Results contained in this section are therefore limited to the Fairbanks/Yellowknife baseline of 1631.1 kilometers.

The test sequence began at 12:40 PM local time and lasted for 2 hours, 50 minutes. Simultaneous measurements were made over a common time interval of two hours. Timetag corrections ranged from 0.0079 milliseconds to 0.055 milliseconds for the Fairbanks data and from 0.175 milliseconds to 6.936 milliseconds for the Yellowknife data.

4.2.2.1 Satellite Geometry, Fairbanks Site - Figure 4-65 shows the satellite geometry for the Fairbanks site. Although the satellite trajectories are very similar to those shown in Figure 4-39 for Fairbanks on Day 208, they do contain minor points of inflection due to missing data. The effects of missing data are much more evident in the DOP measures plotted in Figure 4-66. Here, sharp discontinuities in the otherwide smooth curves result from the loss of 41 data sets (20.5 minutes) between observation numbers 27 and 28. Much smaller discontinuities can be seen due to two missing data sets (1.0 minute) between observations numbers 157 and 158. The reason for the loss of data at the Fairbanks site is unknown.

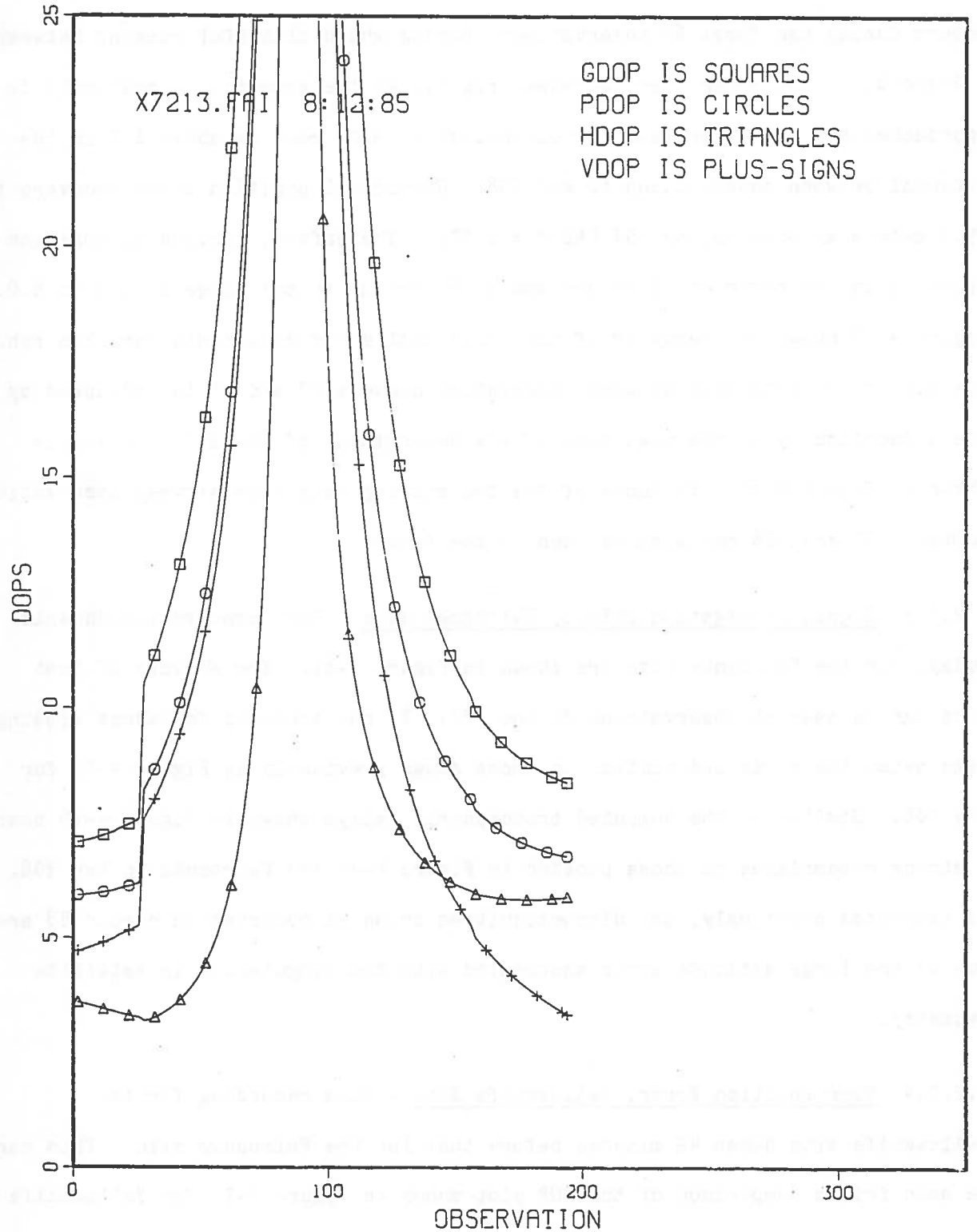

FIGURE 4-66. DILUTION OF PRECISION MEASURES, DAY 213, FAIRBANKS

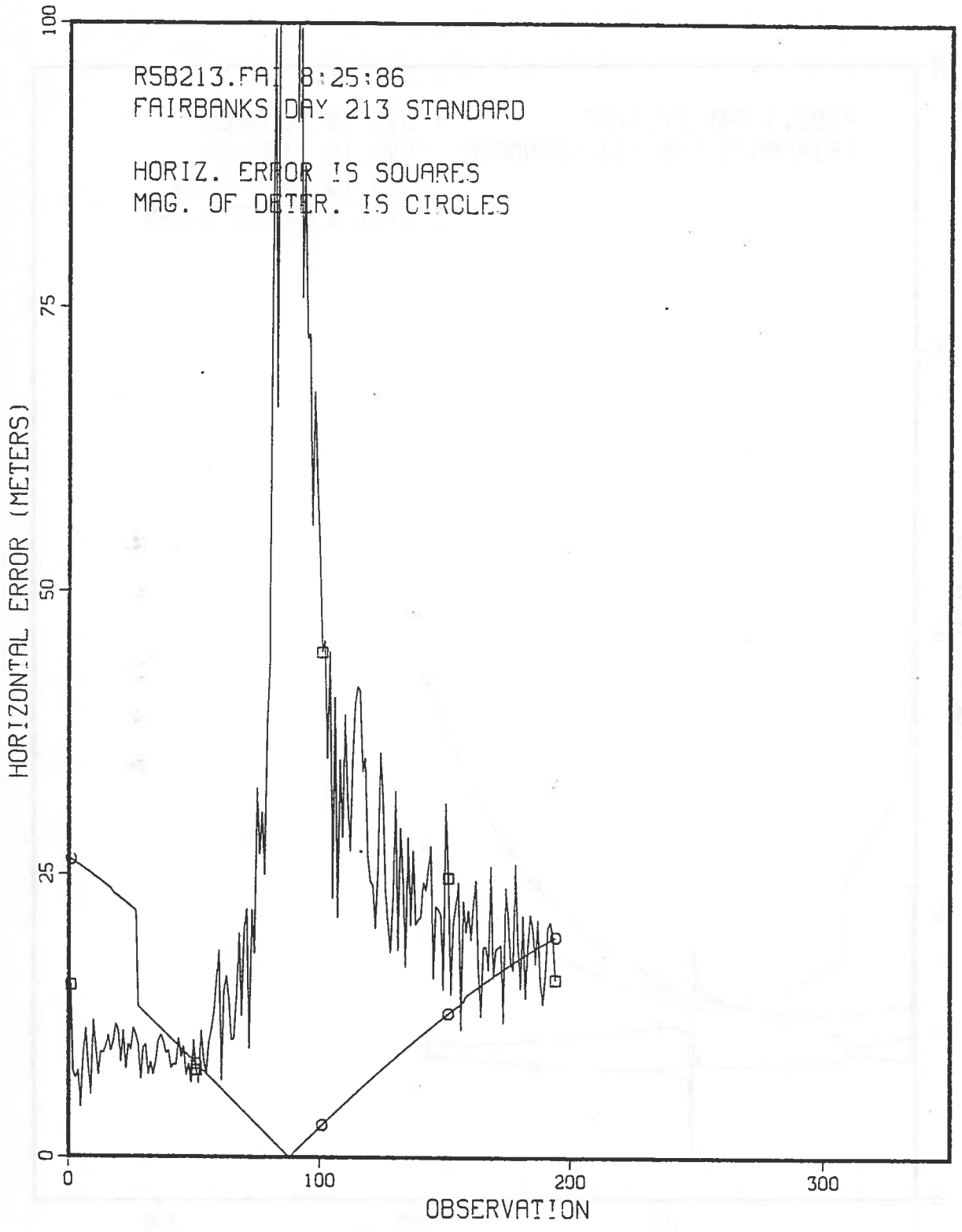

FIGURE 4-67. HORIZONTAL POSITION ERROR, DAY 213, FAIRBANKS

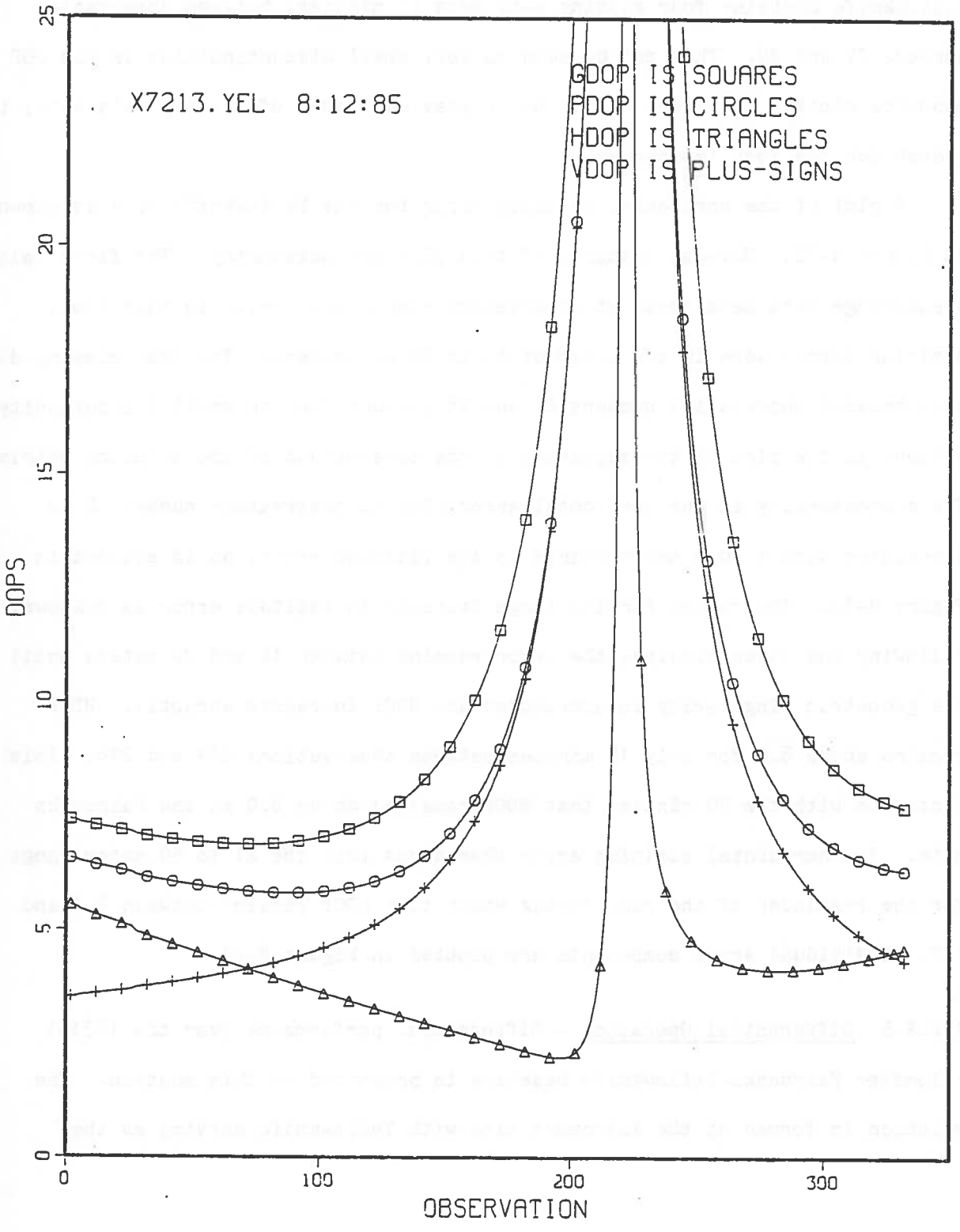

FIGURE 4-71. DILUTION OF PRECISION MEASURES, DAY 213, YELLOWKNIFE

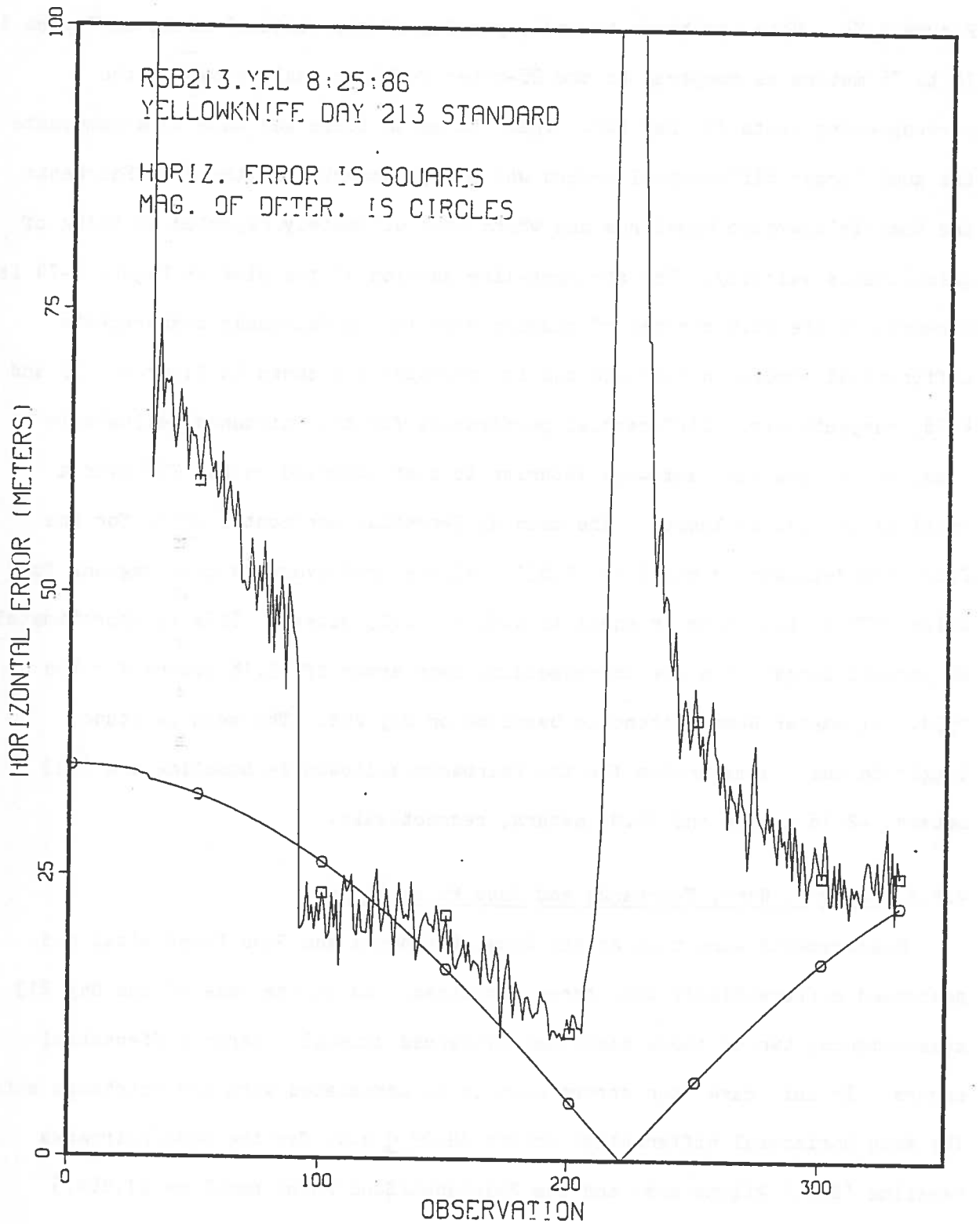

FIGURE 4-72. HORIZONTAL POSITION ERROR, DAY 213, YELLOWKNIFE

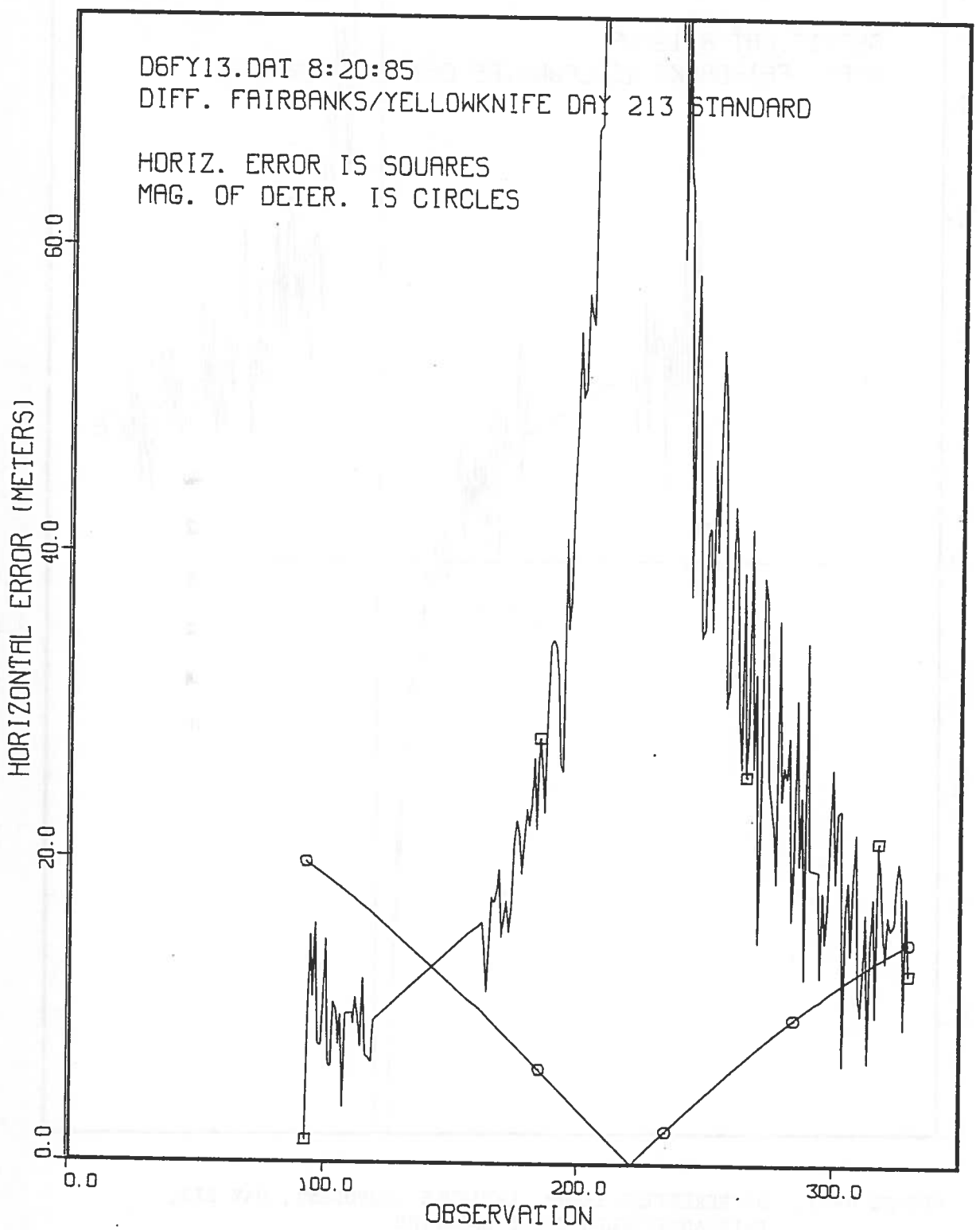

RE 4-74. HORIZONTAL DIFFERENTIAL ERROR, DAY 213, FAIRBANKS/YELLOWKNIFE BASELINE

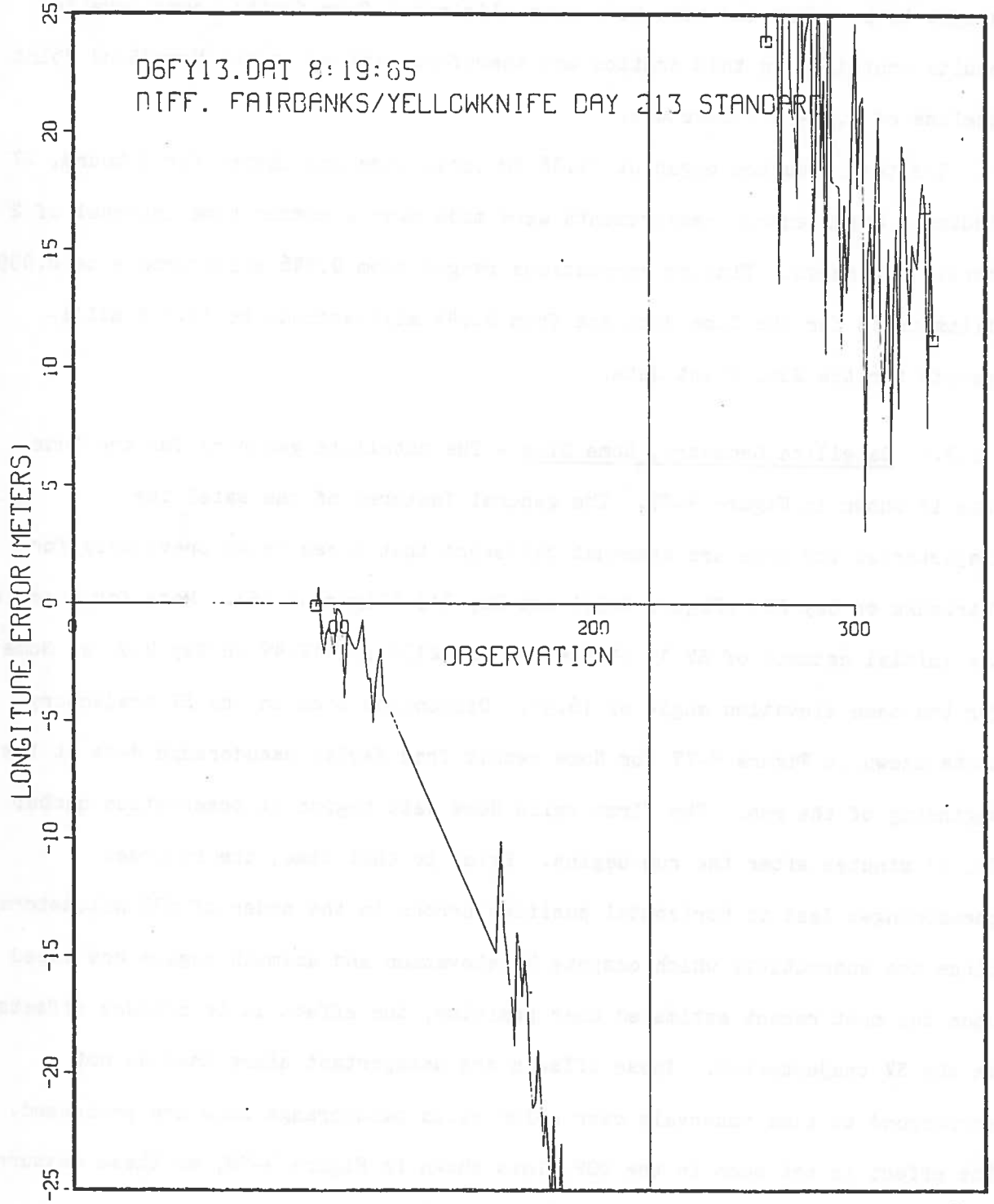

FIGURE 4-76. DIFFERENTIAL ERROR, LONGITUDE COMPONENT, DAY 213, FAIRBANKS/YELLOWKNIFE BASELINE

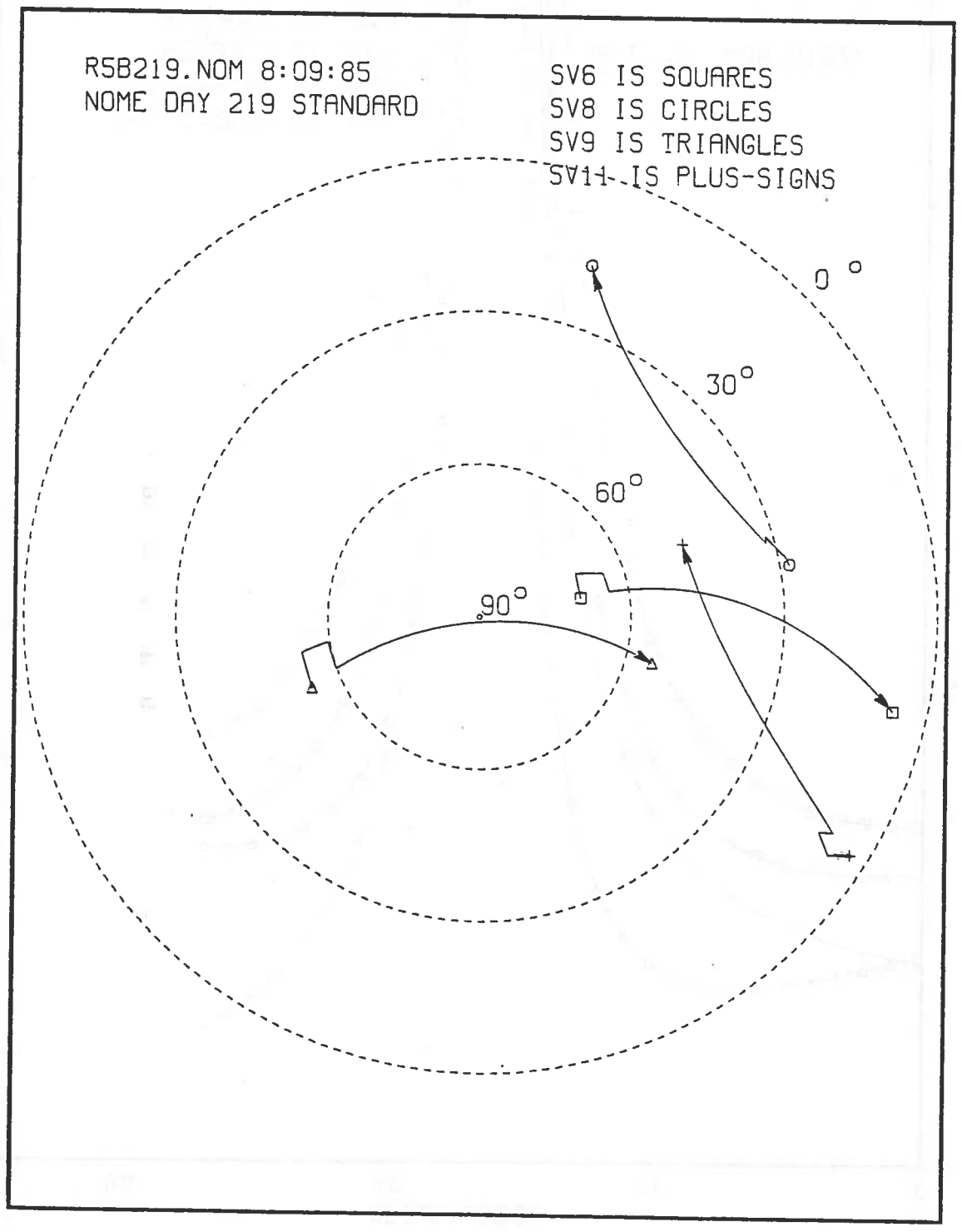

FIGURE 4-77. SATELLITE GEOMETRY, DAY 219, NOME

4.2.3.2 User Position Error, Nome Site - Figure 4-79 shows the horizontal position error for Nome. As mentioned in the previous section, the first valid data occur at observation number 23, at which point the horizontal error drops to 14.3 meters. Thereafter the error trend increases as the geometric singularity (observation number 163) is approached. HDOP remains between 3.6 and 6.0 until observation number 124 is reached and the horizontal position error has increased to 78.4 meters. Horizontal position error recovers after the geometric singularity, falling to 54.4 meters at the end of the run. HDOP remains above 6.0 throughout this latter portion of the run, ending with a value of 6.6. Individual error components are shown in Figure 4-80 where the longitude component can be seen to be the dominant error source.

4.2.3.3 Signal Propagation Delays, Nome Site - The computed ionospheric delays for Nome are shown in Figure 4-81. The discontinuity shown in the plot for SV 11 occurs at observation number 24. This is a result of the invalid data prior to observation number 23. Note that the computation of the ionospheric delay at observation number 24 is based upon the previously computed user position found at observation number 23. As mentioned previously, data prior to observation number 23 are considered invalid and are not used in determining differential error performance.

Plots of the computed tropospheric delays for Nome are shown in Figure 4-82. The effects of invalid pseudorange data prior to observation number 23 are evident. The minor discontinuity evident in the delay for SV 11 results from the loss of two data sets between observation numbers 54 and 55. Discontinuities at observation number 163 result from large altitude errors associated with the singularity in SV geometry occurring at that point.

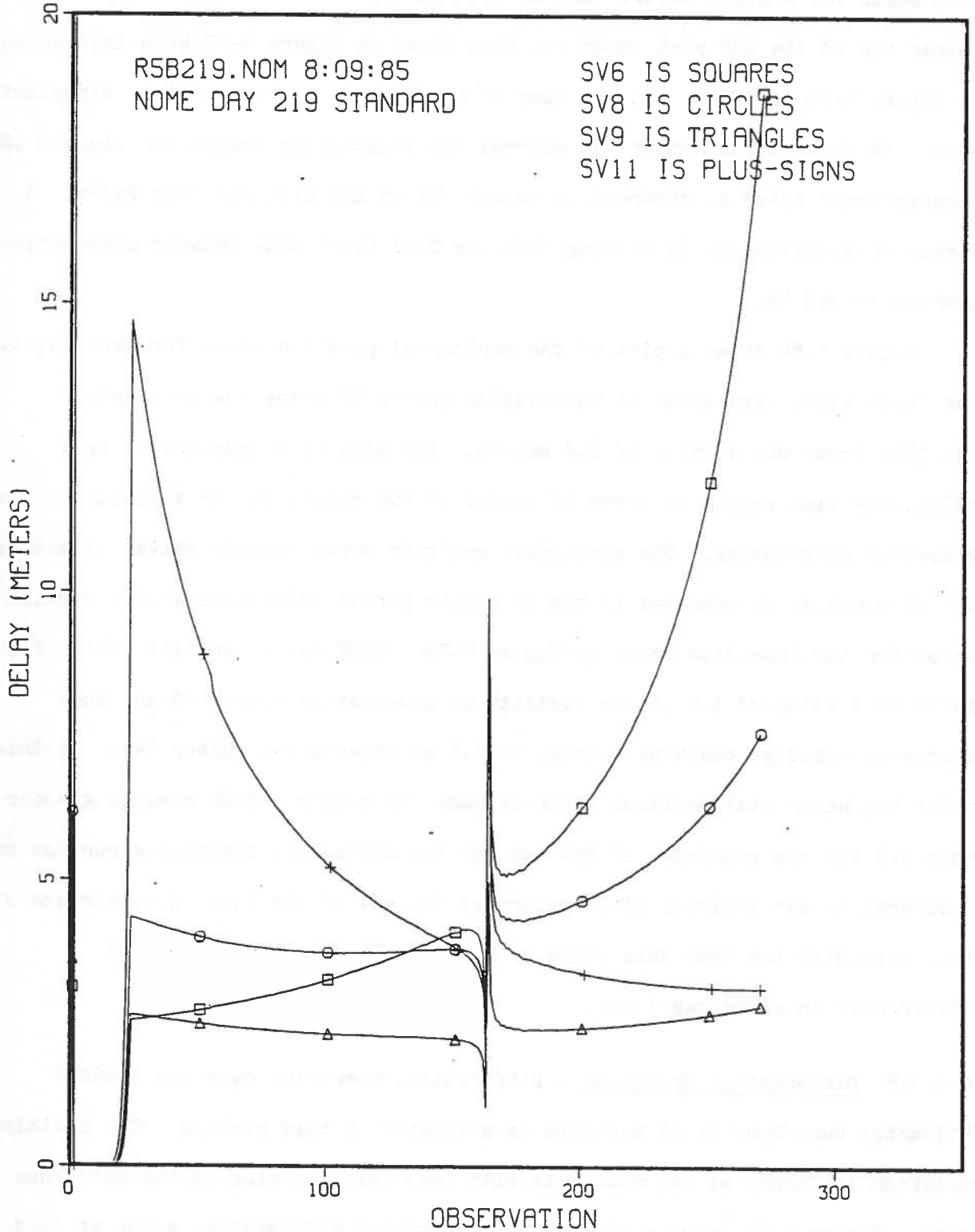

FIGURE 4-82. COMPUTED TROPOSPHERIC DELAY, DAY 219, NOME

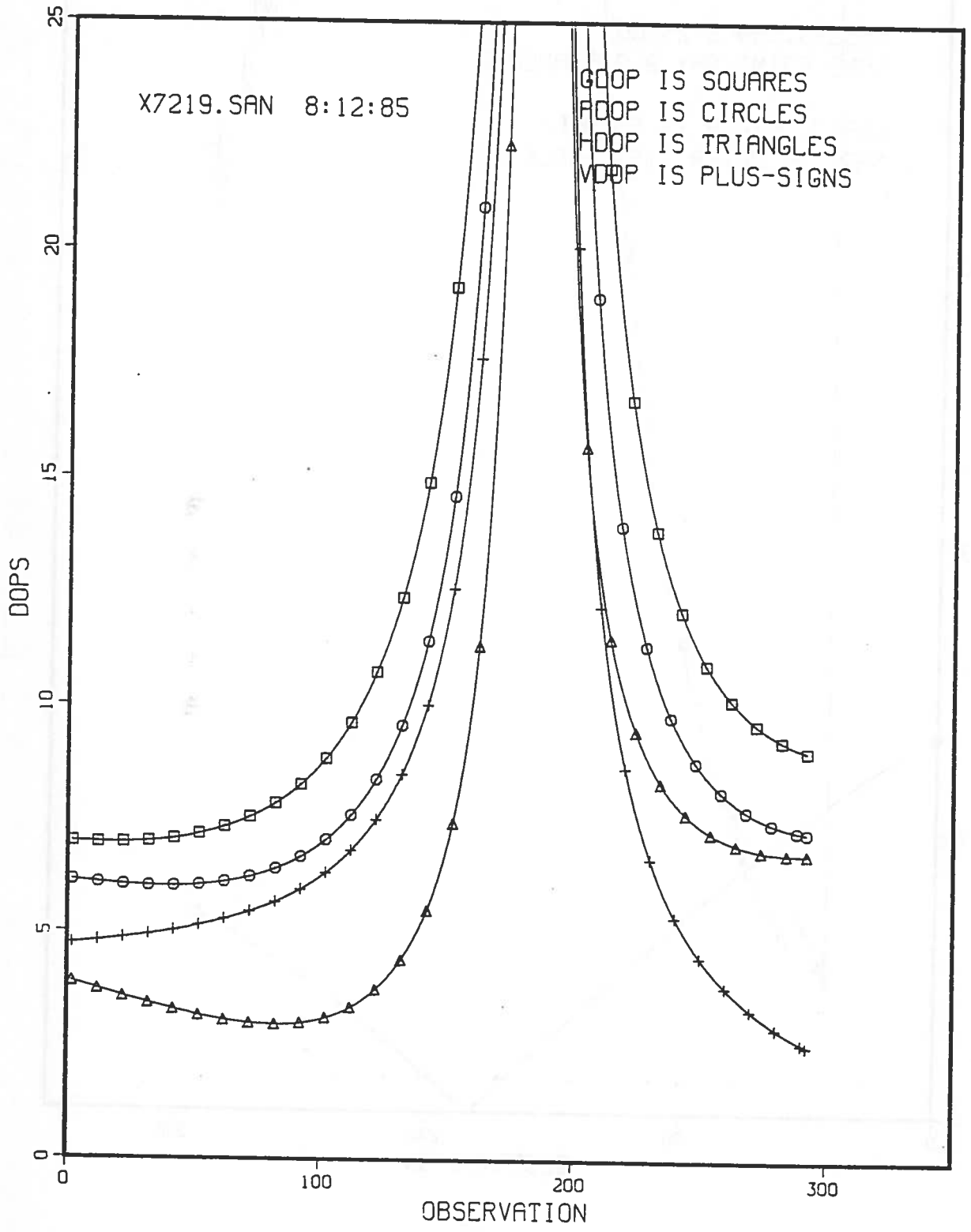

FIGURE 4-83. DILUTION OF PRECISION MEASURES, DAY 219, SAND POINT

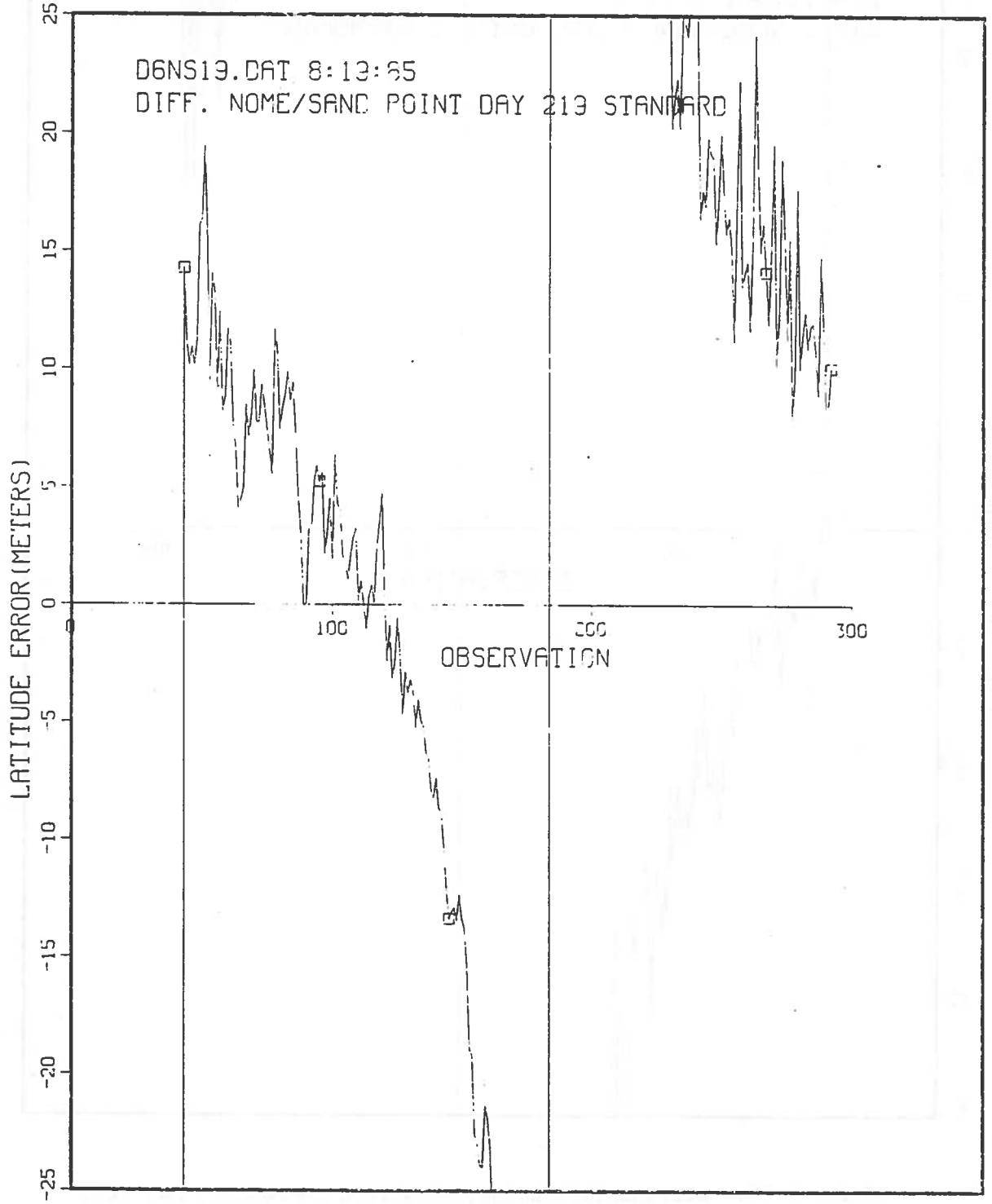

FIGURE 4-87. DIFFERENTIAL ERROR, LATITUDE COMPONENT, DAY 219, NOME/SAND POINT BASELINE

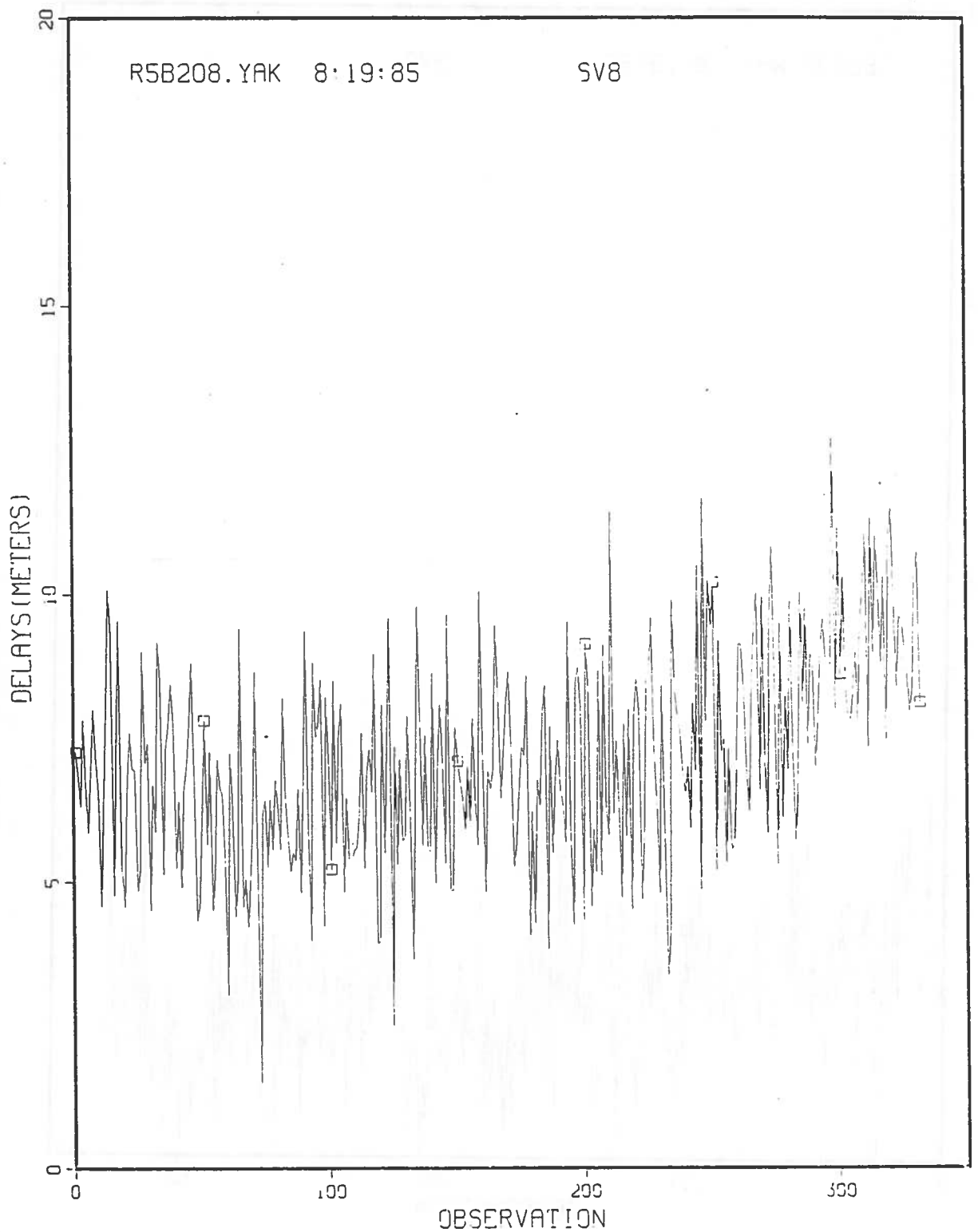

FIGURE 4-89. COMPUTED IONOSPHERIC DELAY, DAY 208, YAKATAGA

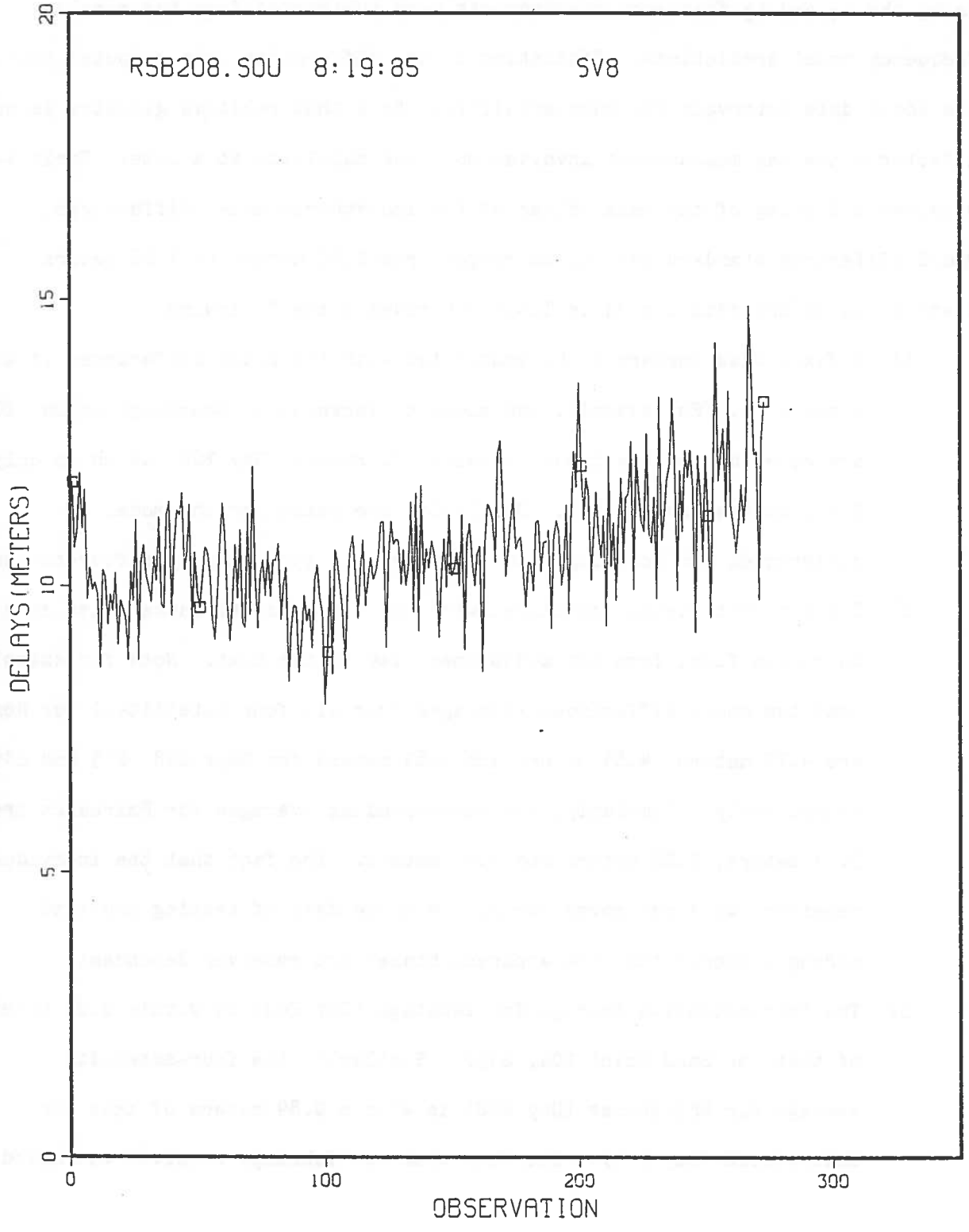

FIGURE 4-91. COMPUTED IONOSPHERIC DELAY, DAY 208, SOURDOUGH

TABLE 4-6. MEAN IONOSPHERIC MODEL DIFFERENCES (METERS)

DAY	SITE	SV-6	SV-8	SV-9	SV-11	FOUR SV AVERAGE
208	NOME	-4.52	-5.16	-3.60	-5.87	-4.79
208	FAIRBANKS	-2.41	-3.76	-2.53	-3.73	-3.11
208	SOURDOUGH	-7.61	-8.80	-7.53	-8.70	-8.16
208	YAKATAGA	-4.15	-4.98	-3.85	-5.36	-4.59
208	WHITEHORSE	-1.00	-1.86	-0.87	-2.23	-1.49
213	NOME	-4.42	-5.04	-3.48	-5.52	-4.62
213	FAIRBANKS	-2.90	-3.87	-2.31	-3.79	-3.22
213	YELLOWKNIFE	-1.89	-2.50	-2.04	-3.09	-2.38
219	NOME	-4.65	-4.81	-3.64	-5.65	-4.69
219	FAIRBANKS	-2.65	-2.91	-2.40	-4.09	-3.01
219	SAND POINT	-4.40	-4.97	-4.10	-5.90	-4.84

5. CONCLUSIONS AND OBSERVATIONS

The following conclusions are drawn from the data analysis presented in this report.

- Differential processing is shown to be an effective method in reducing the effects of bias errors in a GPS system.
- Limited results support the contention that Differential GPS may satisfy the safety requirements for Harbor/Harbor Approach Navigation.
- User/reference site separations of up to 1,000 kilometers may be feasible.
- Mean differential errors tend to follow a linear trend over user/reference site separations ranging from 276 to 1591 kilometers.

The conclusions listed above are based upon a very limited amount of data and hence must be considered tentative. Selective Availability, which is expected to be a major error source, was not present during these tests. Data from the California VLBI site measurements were gathered during periods of darkness when a second major error source, ionospheric delay, is expected to be at a minimum. Ionospheric delays encountered during the Alaska/Canada tests should have been near their daily maximum, however, the measurements were made in summer at high latitudes. Ionospheric delays are expected to reach a seasonal low in the summer and to be relatively small at such high latitudes.

The following points are made with respect to the analysis and the observations listed above.

REFERENCES

1. J.H. Kraemer, "GPS Field Test Data Analysis," TSC Project Memorandum DOT-TSC-CG545-PM-84-38, January 1985.

2. E.E. Altshuler, "Corrections for Tropospheric Range Error," Air Force Cambridge Research Laboratory, Report AFCRL-71-0419, 27 July 1971.

3. J.A. Klobuchar, "Ionospheric Effects on Satellite Navigation and Air Traffic Control Systems," Paper Reprinted from Lecture Series No. 93, Recent Advances in Radio and Optical Propagation for Modern Communications, Navigation and Detection Systems, AGARD, North Atlantic Treaty Organization.

4. "NAVSTAR GPS Space Segment/Navigation User Interfaces," Interface Control Document ICD-GPS-200, Rockwell International Corporation, January 25, 1983.

5. R. Kalafus, et al., "NAVSTAR GPS Simulation and Analysis Program," TSC Report No. DOT-TSC-RSPA-83-11, December 1983.

108 copies